

ALMA MATER STUDIORUM
Università di Bologna

SCUOLA DI SCIENZE
DIPARTIMENTO DI FISICA ED ASTRONOMIA

LAUREA MAGISTRALE IN ASTROFISICA E COSMOLOGIA

**Astrometric and Photometric
characterization of the PRISMA
Fish-eye Cameras for Meteor
Observations**

Relatore:
Prof. Alberto Buzzoni

Laureanda:
Camilla Marcatelli

Co-relatori:
Albino Carbognani
Roberto Di Luca

A.A. 2017 - 2018
III Session

To my family and love

Abstract

The project PRISMA is the first network for systematic surveillance of meteor and atmosphere. More specifically this thesis is about the astrometric and photometric characterization of PRISMA cameras and also the computation of meteoric trajectories. In the first and second chapter there is a general overview of meteor phenomena and a theoretic description of meteoroid interaction with the atmosphere. At the beginning of the third chapter there is a description of the project, what it deals with and who participates. Then there is the general specification of the Basler camera and the tests that have been conducted on a single camera. These tests have been useful to understand how temperature variations could affect the response of the camera and which magnitude the camera works better. In the fourth chapter it can be find the procedure to clean and subsequently to obtain the catalogs from the images taken with the Basler camera. Then it is explained what is the procedure to arrived at an astrometric solution with the software Scamp. Afterwards the obtained results are illustrated. In the last chapter, the dynamic calculation is explained to get the meteoric trajectory from the astrometric images taken from two stations of PRISMA network, Lignan and Torino.

Sommario

Il progetto PRISMA è la prima rete italiana per la sorveglianza sistematica delle meteore e dell'atmosfera. Nello specifico, questa tesi si occupa della caratterizzazione astrometrica e fotometrica delle camere "fish-eye" di PRISMA. Inoltre si calcola la traiettoria di un bolide osservato da due stazioni della rete italiana, Lignan e Torino. Nel primo e secondo capitolo viene data una generale panoramica sui fenomeni meteorici e una descrizione teorica dell'interazione dei meteoroidi con l'atmosfera. Il terzo capitolo è la trattazione del progetto, chi ne fa parte, si descrivono le specifiche generali della camera Basler e i test che sono stati condotti su di essa, utili per capire come le variazioni di temperatura potrebbero influire sulla risposta della camera e in quale magnitudine la camera lavora. Nel quarto capitolo viene spiegata qual è la procedura per ripulire le immagini ottenute con la camera Basler e di seguito come ottenere i relativi cataloghi. Inoltre viene spiegata la procedura utilizzata per realizzare i cataloghi, con il software SExtractor e come arrivare a una soluzione astrometrica con il software Scamp, riportando di seguito i risultati ottenuti. Infine, l'ultimo capitolo verte sul calcolo dinamico al fine di ottenere la traiettoria del bolide utilizzando le immagini di cui è stata fatta la calibrazione astrometrica.

Contents

1	Introduction to meteor phenomena	1
1.1	Meteoroids	1
1.2	The meteor phenomenon	2
1.2.1	Meteors	2
1.2.2	Fireballs, Bolides, Meteorite Falls	2
1.2.3	Explosive Impacts	3
1.2.4	Meteoric dust particles	3
1.3	Meteoroid interaction with the atmosphere	3
1.4	Other phenomena connected with meteors	4
2	Physical Theory of Meteors	6
2.1	Dimensionless numbers and relevant forces	6
2.2	Ablation	7
2.3	Pre- and Post-Ablation Regimes	10
2.3.1	Preheating	10
2.3.2	Dark-Flight and Impact	12
2.4	Integral light	13
2.4.1	ReVelle's differential (Instantaneous) radiation efficiency	16
2.4.2	Integral radiation efficiency	16
2.5	Ionization	17
2.5.1	The Ionization trail formation	17
2.5.2	Initial radius and initial temperature of the ionized trail	18
2.5.3	Dissipation off the Ionization	18
3	PRISMA project	20
3.1	Basler Camera	22
3.2	General specifications	24
3.3	Stress test Results	25
3.4	Photometric characterization	28

4	Astrometric characterization of PRISMA cameras	38
4.1	Cleaning of the images	38
4.2	Astrometric Pipeline	40
4.2.1	Sextractor (Source Extractor)	40
4.2.2	Scamps	59
4.3	Results	71
5	Calculation of meteoric trajectories	74
5.1	Theory for the calculation of fireball trajectory	74
5.2	Triangulation results for two stations	75
5.2.1	Conclusion and future prospective	80
	Bibliography	i

Chapter 1

Introduction to meteor phenomena

When solid particles of the Solar System that are large enough interact with the Earth's atmosphere light is produced, this phenomenon is called a meteor. Following the International Astronomical Union (IAU) nomenclature, the particle will be called meteoroid. Not all the meteoroids are able to produce meteors but it depends on the size and the velocities. The smallest size is about 0.01 mm while large sizes have no limit. Part of the meteoroid population is linked to comets as shower meteors derived from cometary meteoroid streams, another part is linked to asteroids [1]. Some meteoroids may be left directly from the process of formation of larger planetary bodies or as the disintegration of a large cometary body coming in the inner Solar System from the Oort cloud. Moreover others come from the collision between asteroids from the main belt.

1.1 Meteoroids

The knowledge is biased by the condition that the meteoroid orbit must intersect the Earth's orbit. Atmosphere is a large sensor recording the meteoroid impacts upon the Earth. The penetration through the atmosphere may give rise, accordingly to sizes and velocities, to a luminous phenomenon as a meteor, or if brighter, as a meteoric fireball, called also a bolide (for detonating fireballs). Velocities of Solar-System meteoroids at their encounter with the Earth's atmosphere are within the following limits: the lower one 11.2 km/s (only gravity of the Earth), the upper one 72.8 km/s. The direction where the meteoroid comes from is called *radiant*, a term originating from the observation of near parallel trails of meteoroids belonging to one stream: the apparent trails of meteors then belong to the same meteor shower and are seemingly radiating from one point on the sky. Meteors

not belonging to any specific shower are called sporadic meteors. The ability to penetrate the atmosphere is linked to velocities and mass loss due to severe ablation. The term ablation has the meaning of mass loss of a meteoroid in any form and phase: solid as fragments, fluid as droplets and loss of hot gas, which forms always the final stage and is responsible for the observed meteor phenomenon.

1.2 The meteor phenomenon

The penetration of a meteoroid into the Earth's atmosphere at hypersonic velocity gives rise to four different phenomena, depending mostly on mass and partly on velocity. In all types of interaction, ions and free electrons are produced during the atmospheric flight, an ionized column is formed, and forwarding with the meteoroid velocity. This yields a possibility to observe meteor phenomena by radar echoing.

1.2.1 Meteors

Typical meteors are caused by meteoroids larger than about 0.01 mm. The exact size limit depends on velocity. These phenomena are associated with meteoroid sizes between 0.05 mm and 20 cm, entering the atmosphere they are heated up very quickly. The meteoroid can be heated in different ways, if the sizes are between 0.05 mm and 0.5 mm, the body is heated throughout; in the case of a body larger than 0.5 mm, only the surface layer down to a few tenths of a millimeter is heated. At the increasing of the superficial temperature till 2200 K, the sublimation of the superficial material begins so these particles, in form of hot vapors, fill the surrounding of the body. More than 90% of the meteor light originates from radiation of single low-excited atoms of these meteor materials. During the ablation the meteoroid is slowing down and after a certain distance the meteor terminated its light, because it has lost all of its mass.

1.2.2 Fireballs, Bolides, Meteorite Falls

When the size is larger than about 20 cm, it can talk of phenomena like Fireballs, Bolides or Meteorite falls. In this scenario there is not enough time to ablate the entire meteoroid mass, before the body slows down to a critical limit of about 3 km/s. The velocity is too small to maintain a superficial temperature above 2200 K. So the meteoroid cools down and forms a crust on the surface typical for meteorites. Meteoric fireball terminates its light due to small velocity of the meteoroid remnant, whose mass falls down on the Earth in what is called dark flight where the velocity approaches the free fall velocity in a resting medium.

The dark flight lasts typically several minutes in contrast to the fireball luminous trajectory, which lasts for several seconds. A fireball with an absolute mag lower than -17 is called superbolide. For small asteroids of tens of meters in diameter the superbolide can be brighter than the Sun seen from the Earth. An example of such an extreme event is the small asteroid of about 20 meters in diameter exploded at an altitude of about 27 km above the city of Chelyabinsk (Russia) on February 15, 2013 at about $03:20:32.2 \pm 0.1$ s UTC.

1.2.3 Explosive Impacts

This type of phenomenon has a very small probability of happening but it can talk of an explosive impacts when a very large body of several meters has a small deceleration and it hits the Earth's surface before it is slowed down below hypersonic velocity. In this case the meteoroid vapors emit light down to the very contact with the Earth's surface, where an explosive crater forms.

1.2.4 Meteoric dust particles

This phenomenon cannot be observed because it is not luminous. In fact if the size of the meteoroid is less than several hundredths of a millimeter, the body is slowed down very quickly, so it cannot rise its temperature to the evaporation point. Thus the hot vapors are not present, i.e., there is no meteor phenomenon. This meteoroid dust particle is not changed through the atmosphere till reaching the Earth's surface.

1.3 Meteoroid interaction with the atmosphere

In more details, it can be distinguish the following five regimes of meteoroid motion including the orbital motion. The four regimes of the atmospheric motion are: preheating, ablation, dark-flight and impact.

1. Orbital motion

Orbital motion of a meteoroid is dominated by the gravity of our Sun perturbed by close approaches to bigger bodies, i.e. planets. The meteoroid is affected by collisions, irradiation from cosmic rays and other forces.

2. Preheating

Preheating is caused by the impacting molecules of the individual constituents of the air gas, when the body approaches the Earth at heights of 300 to 100 km. There is no time for bodies of even millimeter dimensions to be heated throughout. The preheating is a very quick phenomenon lasting

only few seconds. For bodies larger than 1 mm the process is governed by heat conductivity, while radiation transfer becomes very important for smaller bodies. When the surface tension reaches the strength of the material, spallation starts.

3. Ablation

The next stage is Ablation, it starts as fragmentation (or spallation) at the lower temperatures. After melting the final stage of ablation is the evaporation from the body and from its fragments. The temperatures are close to 2500 K when evaporation starts. The fragmentation process has not been well understood until recently and mostly single body theory has been used. Once ablation starts, it is a severe process and consumes the majority of the kinetic energy. Deceleration can compete with this process in consuming kinetic energy only for larger bodies.

4. Dark Flight

In this part of trajectory ablation ceases because there is not enough kinetic energy to either evaporate, or to provide heating. The process is now inverted, it is a quick cooling. In this moment a thin crust solidifies. Without wind and being decelerated, the body motion changes to vertical trajectory and a free fall follows with velocity decreasing proportionally to square root of the air density. Different wind directions and speeds at different heights perturb the trajectory and complicate the situation, but knowing the wind field, the dark flight trajectory can be computed by numerical integration of the equations of motion and the impact point.

5. Impact

The range of impact velocities are 10 to 100 $m s^{-1}$ for 10 g to 10 kg terminal masses. The impact forms a small pit on the surface but the shape of such pit does not convey any information on the initial motion of meteoroid before entering the atmosphere. However it shows overwhelming direction of winds during the last few kilometers of the dark flight.

1.4 Other phenomena connected with meteors

1. Meteor Flares

Suddenly the brightness of meteor increases by more than one magnitude, this phenomenon is called meteor flare. Typically there are two reasons for this to happen: a fragmentation or a change in physical circumstances increasing evaporation, excitation and ionization.

2. Meteor Wakes

Meteor wakes describes the radiation behind the meteor, while the radiation around the body is called head radiation. There are two types of wakes: the first originates from gas, the second from particulate.

3. Meteor Trains

The meteor train is a radiation emitted behind the head of the meteor for seconds or more.

Chapter 2

Physical Theory of Meteors

2.1 Dimensionless numbers and relevant forces

During the drag phase, only six discrete interaction regimes are possible (ReVelle, 1993) that are listed in table 2.1, created following a model that has unified the study of meteor entry on all size scales but neglected the gross fragmentation process. At high altitudes it can be assumed a free path because the particles collide with the surface of the meteor and it is difficult that after the collision they encountered another particle due to the rarefied flow conditions. The ballistic part of this interaction can be understood in terms of the ratio of the surface pressure of the atmosphere compared to the body's modified ballistic entry parameter, α , as in table 2.1. For small bodies this ratio is quite large indicating that a significant deceleration will occur in the absence of ablation processes, A_e . While for large bodies this ratio will be quite small and consequently also the deceleration will be small, without ablation effects. In the free molecule flow regime, the body's temperature will rise due to collisions and ablation process initiates. At lower altitudes a diffuse shock wave forms as the body begins to ablate and an air cap forms around the front face of the meteoroid shielding it from other impacts. For large bodies decreasing the altitude a radiating fluid blast wave of cylindrical shape forms. This nonlinear zone surrounding the body is the product of the meteoroid's Mach number and its diameter. So the key forces affecting the interaction include that of drag, lift and of the body weight component along the trajectory. Instead the key dimensionless numbers that affect the meteoroid behavior include the Reynolds number, Re (= inertial fluid forces/viscous fluid forces), Mach number, Ma (= body speed with respect to the adiabatic phase velocity of sound waves, c_s), Knudsen number, Kn (= ratio of the neutral gas mean free path to a characteristic body dimension); and for large bodies also the Bouguer number, Bu , and the radiation-convection parameter of an adiabatic shock layer, Γ_{rc} .

Interaction Type	Kn	α	A_e
Thermosphere micro-meteoroid regime	$\gg 1$	$\gg 1$	$\ll 1$
Free molecule flow regime	$\gg 1$	$\gg 1$	$\gg 1$
Transition flow regime	O(1)	> 1	$\gg 1$
Continuum flow regime	$\ll 1$	O(1)	> 1
Impact cratering regime	$\ll 1$	< 1	O(1)
Explosive cratering regime	$\ll 1$	$\ll 1$	$\ll 1$

Table 2.1: Different interaction between meteoroid and atmosphere

2.2 Ablation

By the term "ablation" it can be identified any removal of mass from a meteor body during its passage through the atmosphere, in form of gas, droplets or solid fragments. In the past different models were presented in various articles by Hoppe (1937), Levin (1961) or ReVelle (1979) but all these solutions assumed schematic isothermal atmosphere and found closed mathematical expressions only for velocity as function of time. Instead a new solution to the differential equations of meteoroid motion and ablation was presented by Pecina and Ceplecha (1983, 1984) in the form of $l = l(t)$, i.e., the distance, l , traveled by the body in its trajectory as function of time, t . This solution holds for any atmospheric density profile, it is described below.

The motion and ablation of a single non-fragmenting body through the atmosphere can be represented by three differential equations:

1. the drag equation (2.1);
2. the mass-loss equation (2.2);
3. the height equation (purely geometrical and written for spherical Earth's surface (2.3).

$$\frac{dv}{dt} = -\Gamma A \rho_d^{-2/3} \rho m^{-1/3} v^2 \quad (2.1)$$

$$\frac{dm}{dt} = -\frac{\Lambda A}{2\xi} \rho_d^{-2/3} \rho m^{-2/3} v^3 \quad (2.2)$$

$$\frac{dh}{dt} = \frac{l - A/2}{B/2 + h} v \quad (2.3)$$

$$\frac{A/2 - l}{B/2 + h} = \cos z(t) \quad (2.4)$$

$$Al + Bh + C = l^2 - h^2 \quad (2.5)$$

Equation (2.5) contains constant values A, B, C, which are given by the geometrical relation between distances along the meteoroid trajectory and heights measured from the spherical Earth's surface. This equation can be used as a good check of validity of any set of l and h values for meteors. For any point of a meteoroid trajectory the notation has the following meaning: $v \equiv$ velocity; $t \equiv$ time; $m \equiv$ mass; $h \equiv$ height; $l \equiv$ distance along the trajectory; $\rho \equiv$ air density; $z \equiv$ zenith distance of the radiant; $\Gamma \equiv$ drag coefficient; $\Lambda \equiv$ heat transfer coefficient; $A = Sm^{-2/3}\rho_d^{2/3}$ is the shape factor; $S \equiv$ head cross-section; $\rho \equiv$ bulk density; $\xi \equiv$ energy necessary for ablation of a unit mass. Two independent parameters of the problem can be expressed as the ablation coefficient

$$\sigma = \frac{\Lambda}{2\xi\Gamma} \quad (2.6)$$

and the shape-density coefficient

$$K = \Gamma A \rho_d^{-2/3} \quad (2.7)$$

By keeping σ and K constant, the following integrals of equation (2.1)-(2.3) can be derived:

$$m = m_\infty \exp\left(\frac{1}{2}\sigma[v^2 - v_\infty^2]\right) \quad (2.8)$$

where $m \rightarrow m_\infty$, $v \rightarrow v_\infty$, for $t \rightarrow -\infty$ (outside the atmosphere). By substitution of (2.8) into (2.1) and integrating the velocity integral is obtained:

$$Ei\left(\frac{1}{6}\sigma v_\infty^2\right) - Ei\left(\frac{1}{6}\sigma v^2\right) = \frac{2K \exp\left(\frac{1}{6}\sigma v_\infty^2\right)}{m_\infty^{1/3}} \int_h^\infty \frac{(B/2 + h)\rho dh}{(A^2/4 + C + h^2 + Bh)^{1/2}} \quad (2.9)$$

The integral relating velocity to time is

$$t - t_0 = \int_{l_0}^l \frac{dl}{v} \quad (2.10)$$

and the integral relating height and distance along the trajectory to time is

$$\frac{Ei\left(\frac{1}{6}\sigma v_\infty^2\right) - Ei\left(\frac{1}{6}\sigma v^2\right)}{Ei\left(\frac{1}{6}\sigma v_\infty^2\right) - Ei\left(\frac{1}{6}\sigma v_0^2\right)} = \frac{\int_h^\infty \frac{(B/2+h)\rho dh}{(A^2/4+C+h^2+Bh)^{1/2}}}{\int_{h_0}^\infty \frac{(B/2+h)\rho dh}{(A^2/4+C+h^2+Bh)^{1/2}}} \quad (2.11)$$

where the relation of height to distance is given by

$$h = -B/2 + \sqrt{B^2/4 - C + l^2 - Al} \quad (2.12)$$

Here $Ei(x)$ is the exponential integral function, given by

$$Ei(x) = \int_{-\infty}^x \frac{e^x}{x} dx \quad (2.13)$$

v is defined by (2.10) and $v = v_0$, $h = h_0$, $l = l_0$ holds for $t = t_0$. Any point of the trajectory can be defined as $t_0 = 0$: this defines from where it is started to count the relative time t . These integrals hold for any air density profile. Equations (2.10) and (2.11) represent the complete solution of the problem of the single non-fragmenting body with constant coefficients σ and K , and express the distance along the trajectory and the height as function of time, if the four parameters, l_0 , v_0 , v_∞ , σ , are known.

The problem contains four unknown parameters l_0 , v_0 , v_∞ , σ , to be determined from observations. The problem can become linear by writing it for small increments of the parameters. The partial derivatives of (2.10) and (2.11) with respect to all four unknown parameters are explicit analytical expressions, as follows.

$$l_{obs} - l = \frac{\partial l}{\partial l_0} \Delta l_0 + \frac{\partial l}{\partial v_0} \Delta v_0 + \frac{\partial l}{\partial v_\infty} \Delta v_\infty + \frac{\partial l}{\partial \sigma} \Delta \sigma \quad (2.14)$$

$$\frac{\partial l}{\partial l_0} = \frac{1}{v_0 D} 2v \exp\left(\frac{1}{6}\sigma v^2\right) \int_{h_0}^{\infty} \frac{\rho dh}{\cos z} + v_0 v^2 \left[Ei\left(\frac{1}{6}\sigma v_\infty^2\right) - Ei\left(\frac{1}{6}\sigma v^2\right) \right] \varrho(h_0) \int_{l_0}^l \frac{dl}{v^2} \quad (2.15)$$

$$\frac{\partial l}{\partial v_0} = \frac{2v^2}{v_0 D} \exp\left(\frac{1}{6}\sigma v_0^2\right) \int_h^{\infty} \frac{\rho dh}{\cos z} \int_{l_0}^l \frac{dl}{v^2} \quad (2.16)$$

$$\frac{\partial l}{\partial v_\infty} = -\frac{2v^2}{v_\infty D} \exp\left(\frac{1}{6}\sigma v_\infty^2\right) \left[\int_h^{\infty} \frac{\rho dh}{\cos z} - \int_{h_0}^{\infty} \frac{\rho dh}{\cos z} \right] \int_{l_0}^l \frac{dl}{v^2} \quad (2.17)$$

$$\frac{\partial l}{\partial \sigma} = \frac{2v^2}{\sigma D} \int_{l_0}^l \frac{dl}{v^2} \left[\exp\left(\frac{1}{6}\sigma v_0^2\right) \int_h^{\infty} \frac{\rho dh}{\cos z} - \exp\left(\frac{1}{6}\sigma v_\infty^2\right) \int_h^{h_0} \frac{\rho dh}{\cos z} - \exp\left(\frac{1}{6}\sigma v_0^2\right) \int_h^{\infty} \frac{\rho dh}{\cos z} \right] \quad (2.18)$$

where the denominator D is given by

$$D = 2 \exp\left(\frac{1}{6}\sigma v^2\right) \int_{h_0}^{\infty} \frac{\rho dh}{\cos z} + v^2 \left[Ei\left(\frac{1}{6}\sigma v_\infty^2\right) - Ei\left(\frac{1}{6}\sigma v_0^2\right) \right] \varrho(h) \int_{l_0}^l \frac{dl}{v^2} \quad (2.19)$$

Continuous fragmentation can also be treated using this solution, because of the general definition of the ablation coefficient in the single-body model: ablation means just removal of mass in any form, either gas, or fluid and or solid fragments. If the body fragments suddenly at a point, the solution is no longer valid, but it can be generalized in this respect. The simplest model with only one point of gross-fragmentation during the entire atmospheric trajectory, is the same as given by equations (2.10) and (2.11), except that the integration is in two steps and thus there are two additional parameters, so six parameters has to be determined from observations. If gross-fragmentation point is located at $t = t_0$, then

$$l_{obs} - l = \frac{\partial l}{\partial l_0} \Delta l_0 + \frac{\partial l}{\partial v_0} \Delta v_0 + \frac{\partial l}{\partial v_{\infty_1}} \Delta v_{\infty_1} + \frac{\partial l}{\partial \sigma_1} \Delta \sigma_1 + \frac{\partial l}{\partial v_{\infty_2}} \Delta v_{\infty_2} + \frac{\partial l}{\partial \sigma_2} \Delta \sigma_2 \quad (2.20)$$

which is a linear equation analogical to (2.14), except it contains the following six unknown increments of parameters to be determined from observations:

- $\Delta v_{\infty_1}, \Delta \sigma_1$ before fragmentation
- $\Delta l_0, \Delta v_0$ at fragmentation
- $\Delta v_{\infty_2}, \Delta \sigma_2$ after fragmentation

Partial derivatives in (2.20) are again explicit analytical expressions as in the non-fragmentation case (2.14), in complete analogy. Equations (2.17) and (2.18) have to be written with two subscripts: one is valid before the fragmentation point and the other is valid after the fragmentation point. The computational procedure is analogical to that described above equation (2.14).

In case of more fragmentation points, the situation is not so simple. Each additional fragmentation point adds four parameters, if the relative amount of fragmented mass and the position of fragmentation points are also taken as unknowns. Large meteor bodies, especially the meteorite dropping fireballs can reach a maximum deceleration point on their luminous trajectory, that can be written, with the suffix *md* (maximum deceleration), as

$$\left(\frac{dv}{dt} \right)_{md} = -\frac{1}{2} b \cos z_R \frac{v_{md}^2}{1 - \frac{1}{6} \sigma v_{md}^2} \quad (2.21)$$

2.3 Pre- and Post-Ablation Regimes

2.3.1 Preheating

Before the ablation process starts it can be defined a pre-regime, called pre-heating. This part of the atmospheric trajectory can be described by partial

differential equation expressing the flow of energy from the meteoroid surface inside and outside. The energy input originates from the air atoms and molecules hitting the gas-cap-unprotected meteoroid surface directly. The surface temperature at which ablation begins should fall somewhere between the meltin and the boiling points for the body. So it has to be determined at what height this temperature is reached for a homogeneous sphere with radius r_0 , density δ , specific heat c , and heat conductivity λ , assuming black-body radiation. Taken a randomly oriented, rapidly rotating meteoroid whose kinetic energy is converted to heat uniformly distributed on its surface. The following differential equation of heat conduction applies:

$$\frac{\partial \tau}{\partial t} - \frac{2\beta^2}{r} \frac{\partial \tau}{\partial r} - \beta^2 \frac{\partial^2 \tau}{\partial r^2} = 0 \quad (2.22)$$

where $\tau(r, t)$ is the temperature relative to T_0 , as function of time t and distance from the center of the body r ; T_0 is the absolute temperature of the meteoroid outside the atmosphere; σ is Stefan-Boltzman constant; Λ is the heat transfer coefficient; v is the meteor velocity; ϱ is the air density; ϱ_B is the air density at which the meteoroid attains temperature τ_B at surface; b is the air density gradient; z_R is the zenith distance of the radiant; τ_0 is the temperature at the meteoroid center, when the surface temperature is τ_B and

$$\beta^2 = \frac{\lambda}{\delta c} \quad (2.23)$$

$$\tau = \tau(r, t) = T - T_0 \quad (2.24)$$

The initial condition can be written as

$$\tau(r, -\infty) = 0 \quad (2.25)$$

The boundary conditions are:

$$\tau(0, t) = \text{finite value} \quad (2.26)$$

and

$$\lambda \left(\frac{\partial \tau}{\partial r} \right)_{r=r_0} + \sigma(\tau + T_0)^4 - \sigma T_0^4 = \frac{\Lambda \varrho v^3}{8} \quad (2.27)$$

Equations (2.22) and (2.25) assume a more suitable form under the following transformation

$$u = \tau r \quad (2.28)$$

Obtaining

$$\frac{\partial u}{\partial t} - \beta^2 \frac{\partial^2 u}{\partial r^2} = 0 \quad (2.29)$$

and

$$u(r, -\infty) = 0 \quad (2.30)$$

with the relative temperature of the meteoroid surface τ_B at the time $t = 0$. In search of the point where the surface temperature reaches the ablation temperature and so ablation starts. This temperature is somewhere between 2200 K and 2600 K depending on the meteoroid material.

For bodies larger than 1 mm, the radiation term in equation (2.27) can be omitted and the problem becomes linear. The solution is

$$\varrho_B = \frac{8\lambda\tau_B}{\Lambda v^3} \left[\frac{Q}{\beta} \coth \left(\frac{r_0 Q}{\beta} \right) - \frac{1}{r_0} \right] \quad (2.31)$$

with $Q = \sqrt{bvcosz_R}$ and the temperature in the center of the body is given by

$$\tau_0 = \frac{\Lambda v^3 r_0^2 Q \varrho_B}{8\lambda \left[r_0 Q \cosh \left(\frac{r_0 Q}{\beta} \right) - \beta \sinh \left(\frac{r_0 Q}{\beta} \right) \right]} \quad (2.32)$$

2.3.2 Dark-Flight and Impact

If a fireball penetrates very deep into the atmosphere, there might be the possibility to predict a meteorite fall. What is interesting to predict is the impact point from data on the luminous trajectory of the fireball. After terminating the luminous trajectory, the body continues in its flight without emitting light in what is called a dark-flight trajectory. The last measured velocity and deceleration at the terminal point, the position of the terminal point and the direction of flight completely define the solution of this problem. One of the complications in the computations of the dark flight lies in the poorly known wind field. The main uncertainty originates from the unknown shape of the body, which here is assumed symmetrical. The equations of motion of a non-ablating body can be written as

$$\frac{dv_l}{dh} = -\Gamma S \varrho v (V_l + v_l) / v_h \quad (2.33)$$

$$\frac{dv_h}{dh} = (-\Gamma S \varrho v v_h - g) / v_h \quad (2.34)$$

$$\frac{dv_x}{dh} = -\Gamma S \varrho v (V_x + v_x) / v_h \quad (2.35)$$

where v , the velocity of a meteoroid is composed of three perpendicular components: the vertical plane containing the fireball trajectory contains the horizontal component of the velocity, v_l ; the same vertical plane contains the vertical velocity component, $v_h = dh/dt$; the horizontal direction perpendicular to the vertical

plane containing the fireball trajectory contains the other horizontal component of velocity, v_x (perpendicular to the fireball trajectory in horizontal direction). The sign of the velocity components are chosen so that $v_l > 0$ up (in the real problem of the meteoroid motion $v_h < 0$ always), and so that $v_x > 0$ to the right hand side viewing along the meteor motion. The other symbols are: V_l, V_x the wind velocity components, $V_l > 0$ against the meteoroid motion, $V_x > 0$ against the positive direction of v_x ; Γ the drag coefficient as function of Mach number $\Gamma = \Gamma(M)$ (and thus function of v and the air temperature); $S = m/s$ the ratio of meteoroid mass, m , and meteoroid head cross-section, s ; ρ the air density.

The solution of differential equations (2.33), (2.34), (2.35) can be performed numerically starting from the terminal point and going to lower and lower heights until the surface of the Earth is reached (Runge-Kutta method can be used). The air densities for low penetrating fireballs are usually available from meteorological aeronomical measurements. The wind direction and velocity are given from aeronomical data and it is usually taken the closest values in time and location of the fireball and interpolate.

2.4 Integral light

Another important feature to study is the light emitted by the meteoroid during its flight. Because it can be useful to obtain the meteoroid's initial mass and its mass loss along the trajectory, due to a fraction of the meteoroid kinetic energy is transformed into radiation during the flight. So it can be written

$$I = \tau \frac{dE_k}{dt} \quad (2.36)$$

where I is the meteor luminosity, E_k is the meteoroid kinetic energy and τ is the luminous efficiency. In most cases, the energy loss is dominated by ablation which leads to the classical luminous equation relating mass loss (ablation) and luminosity:

$$I = -\tau \frac{v^2}{2} \frac{dm}{dt} \quad (2.37)$$

In general, however, the term of energy loss due to deceleration should be included:

$$I = -\tau \left(\frac{v^2}{2} \frac{dm}{dt} + mv \frac{dv}{dt} \right) = -\tau \left(1 + \frac{2}{\sigma v^2} \right) \frac{v^2}{2} \frac{dm}{dt} \quad (2.38)$$

The ratio of deceleration from equation (2.1) and mass-loss from equation (2.2) are used and σ is the ablation coefficient. The term $2/(\sigma v^2)$ is important for slow meteors with a small ablation coefficient.

The luminous efficiency is by no means a constant, it depends on many parameters. Before discussing the values of τ , it will be discussed its units. In equation (2.36), τ is dimensionless and I is given in energetic units ($ergs^{-1}$) $\equiv (10^{-7} \text{ W})$, i.e., the luminosity is taken to be the total energy emitted across the whole electromagnetic spectrum. In practice, meteors are observed in a limited spectral region and their brightness is usually expressed in absolute (100 km distance) magnitudes, M , as determined through comparison with stars. The magnitude-based luminosity can be defined as

$$I_V^* = 10^{-0.4M_V} \quad (2.39)$$

For luminosity defined in this way, the system in which the magnitude is measured must be specified. In V-band magnitude, the corresponding luminous efficiency is τ_V^* in units (0 mag erg^{-1} s). If I_V^* and τ_V^* are known, the luminous equation can be used with these quantities. However, for a theoretical considerations it is useful to know the conversion to the energetic units. The conversion factor generally depends on the meteor spectrum. A meteor spectrum can be described by the function I_ν , the intensity of meteor radiation ($erg s^{-1} cm^{-2} ster^{-1} Hz^{-1}$) at frequency ν . It is given by

$$I_\nu = B_\nu(T)(1 - e^{-\eta_\nu}) \quad (2.40)$$

Where $B_\nu(T)$ is the Planck function at temperature T and η_ν is the optical depth at frequency ν .

Assuming for simplicity that the meteor is of spherical shape of radius r , then its total luminosity is

$$I = 4\pi r^2 \int_0^\infty I_\nu d\nu \quad (2.41)$$

The filling factor $f_{\nu_1}^{\nu_2}$ between frequencies ν_1 and ν_2 is defined as

$$f_{\nu_1}^{\nu_2} = \frac{\int_{\nu_1}^{\nu_2} I_\nu d\nu}{\int_{\nu_1}^{\nu_2} B_\nu d\nu} \quad (2.42)$$

$f_{\nu_1}^{\nu_2}$ is always ≤ 1 . It is clear that for small intervals of frequencies the filling factor will be very different depending on which lines are present inside the interval. However, for wide passbands in case of bright meteors which contain a lot of randomly distributed lines, the filling factors will be very similar and will converge to the global filling factor f_0^∞ (further denoted as f). Using the filling factor, the total luminosity can be written as

$$I = 4\pi r^2 f \int_0^\infty b_\nu(T) d\nu = r^2 f a c T^4 \quad (2.43)$$

where $a = 7.65 \times 10^{-15} \text{ erg cm}^{-3} K^{-4}$ is the radiation constant. This equation could in principle be used, if T , r and f are estimated from the meteor spectrum.

However, in most cases, only the meteor magnitude is known. If the meteor is observed from the distance R , the radiation flux is

$$F_\nu = \pi I_\nu \left(\frac{r}{R} \right)^2 \quad (2.44)$$

The magnitude M_V is given by:

$$M_V = -2.5 \log \left(\int_0^\infty V_\lambda F_\lambda d\lambda \right) - 13.74 \quad (2.45)$$

where F_λ is given in $\text{erg cm}^{-2} \text{s}^{-1} \text{\AA}^{-1}$ and V_λ is the V filter passband. Using equation (2.44) and (2.45) for $R = 100 \text{ km}$, it can be obtained

$$I_V^* = 9.84 \times 10^{-9} r^2 f \int_0^\infty v_\lambda B_\lambda(T) d\lambda \quad (2.46)$$

and the ratio of physical to magnitude-based intensities is

$$\frac{I}{I_V^*} = \frac{2.30 \times 10^4 T^4}{\int V_\lambda B_\lambda(T) d\lambda} \quad (2.47)$$

To determine the actual values of the luminous efficiency, the mass loss rate dm/dt is needed for some meteors independently of the photometry. From a good quality fireball spectrum, the mass loss, m_G , of meteoric vapors in the radiating volume (of the main spectrum) can be derived. This is done by correcting unobservable elements using the known or assumed chemical composition of the meteoroid. However, this tells nothing about the mass loss rate because the time, the evaporated atoms spend in the radiating volume, is unknown. This time was called the relaxation time, t_R , by Ceplecha (1973). The mass loss rate is then

$$\frac{dm}{dt} = \frac{m_G}{t_R} \quad (2.48)$$

The upper limit of the relaxation time for a particular meteor can be estimated from the duration of meteor flares.

In principle, the mass as a function of time can also be obtained from the solution of meteor motion (the dynamic mass). However, the solution depends on the assumed drag coefficient, shape factor and bulk density. Therefore, to estimate the mass changes we have to know either the initial or the terminal mass of the meteoroid. This has been possible only for artificial meteors and for photographed meteorite falls.

2.4.1 ReVelle's differential (Instantaneous) radiation efficiency

The differential power relation utilized in ReVelle (1980) was that developed earlier by ReVelle and Rajan (1979), with τ_{cfv} , the differential (instantaneous) luminous efficiency, P_L , the instantaneous light power produced over all wavelengths and E_k , the source kinetic energy, and M_P , the photographic stellar magnitude (with the traditional 'color' index = -2 assumed) in the form:

$$P_L = -\tau_{cfv} \frac{dE_k}{dt} = 10^{-0.4(M_P+2)+9.72} \quad (2.49)$$

For many years this type of relationship was used to compute the so-called photometric mass of meteors using an empirically-based differential luminous efficiency value (Ceplecha and McCrosky, 1976), but with the power loss resulting solely from an entry with negligibly small deceleration ($dv/dt = 0$). ReVelle and Rajan used this relation in combination with the entry dynamics model of ReVelle to compute the differential luminous efficiency of the three photographed and recovered chondritic meteorites with available data at that time. ReVelle named it *radiation efficiency* rather than the more conventional term luminous efficiency in order to emphasize the very broad wavelength range considered so that a correct interpretation could still be made by the conventional observers of meteors and meteor-fireballs.

2.4.2 Integral radiation efficiency

ReVelle used the integral of the light produced over all wavelengths compared to the total power output of a bolide at its conventional end height, i.e., where the bolide is no longer luminous to the eye or to its photographic recording, in order to compute this quantity. If the direct connection is made between power output from a bolide and the light produced by the interaction with the atmosphere over all possible radiative wavelengths, then the inverse of the ratio of these two components as evaluated over the entire flight that was defined by ReVelle (1980) to be the integral radiation efficiency of the bolide. This was accomplished assuming that the decay of the meteoroid kinetic energy could be uniquely separated in the form:

$$E_k = E_{k\infty} \exp(-D); \quad D = \alpha + \beta \quad (2.50)$$

The term involving α accounts for kinetic energy depletion due to ablative processes, whereas the term involving β accounts for energy removal due to air drag processes. Using the definitions of the efficiencies of light, heat, ionization and of compressional (acoustical) waves, ReVelle was able to formulate an integral radiation efficiency of light production, τ_L , in term of P_L , the light power radiated in a specified

electromagnetic passaband, E_∞ , the initial kinetic energy and E_E , the terminal value of the kinetic energy and t is time along the trajectory as

$$\tau_L = \frac{\int PLdt}{E_\infty - E_E} \quad (2.51)$$

This approach led to other papers which culminated in the complete numerical solution to the problem in ReVelle (1993) and not the earlier analytic approach described above, which was only 'exact' in the limit of $\sigma v^2/2 \lesssim 6.25$, with σ being the ablation coefficient.

2.5 Ionization

2.5.1 The Ionization trail formation

The ionization produced by inelastic collisions of the vaporized atoms of a meteoroid with air molecules can be described in term of the rate of loss of mass of the meteoroid and the number of free electrons, β , produced per vaporized meteor atom. The number of electrons produced per meter from a meteoroid of mass m , moving with speed V , is

$$q = -\frac{\beta}{\mu V} \frac{dm}{dt} \quad (2.52)$$

where μ is the average mass of an ablated meteoroid atom. The quantity β depends strongly on the relative speed in an atom - molecule collision for $V > 35 \text{ km s}^{-1}$, and can be written $\beta = \beta_0 V^n$, where n lies between 3 and 4. A comprehensive survey by Bronshten (1983) of the quantities involved in this expression, led to $\beta_0 = 3.02 \times 10^{-17}$, $n = 3.42$, when V is in m s^{-1} . For $V < 35 \text{ km s}^{-1}$, Jones (1997) has developed the following expression for the ionization coefficient of faint radio meteors: $\beta = 9.4 \times 10^{-6} (v - 10)^2 v^{0.8}$, where the value of v is in km s^{-1} . Following Love and Brownlee (1991), the value of the mean atomic mass of the evaporated atoms is taken as 40.

From a comparison of simultaneous visual and radar observations of meteors Kaiser (1953) found that a trail with q electrons per meter is related to its visual magnitude M by the formula, $M = 40.0 - 2.5 \log q$. This formula is valid for trails formed by meteoroids with velocities of about 40 km s^{-1} . McKinley (1961) suggests that a more general expression is $M = 36 - 2.5(\log q - \log V)$ where V is the velocity in km s^{-1} . The height of maximum ionization for a faint meteor can be determined from ablation theory.

2.5.2 Initial radius and initial temperature of the ionized trail

Collisions reduce the thermal velocity of the ionized meteor atoms to ambient values in a time less than a millisecond at 100 km. Estimates of the initial radius of the plasma column have been determined both theoretically and experimentally. Theoretical analysis of collision cooling indicates that the initial radius, r_0 can be expressed as $\rho^a v^b$, where ρ is the density of the atmosphere, $a \sim -1$, and $b \sim 0.8$. However, Öpik (1958) and Hawkes and Jones (1975) suggested that continuous fragmentation of rotating dust-ball type meteoroids will produce a lateral spread of ablating particles and hence increase the initial radius. This effect opposes the tendency for the radius to vary as ρ^{-1} . Using a computer simulation based on collisions between elastic spheres, Jones (1995) showed that the ablated ions reach thermal equilibrium after about 10 collisions, and he defined the initial radius r_0 at this time as the r.m.s. value of the radial positions of the ions. He also found that the initial ionization distribution is not Gaussian but has a higher density core of radius of the order $0.4 r_0$ immersed in a more diffuse distribution. The value of r_0 varies as ρ^{-1} . Moreover Jones partially resolved the inconsistency between theory and experiment by estimating an 'effective initial radius', $r_{0(eff)}$, that is obtained when the theoretical non-Gaussian trail is assumed to scatter radio waves as if it had a Gaussian radial distribution of ionization.

2.5.3 Dissipation off the Ionization

After the trail is formed the electron concentration will decrease because of ambipolar diffusion, atmospheric turbulence, and loss of ionization through recombination and ionic reactions. The whole trail will also be subject to large scale wind shears that cause bending and twisting of the original highly linear column. Based on radio studies of meteors, the most important dissipation factor is ambipolar diffusion, which reduces the volume density without affecting the line density. At heights below 90 km, where the effect of the Earth's magnetic field on the diffusing plasma may be ignored, the volume density of electrons (and ions) at time t and distance r from the column axis is described by the radial diffusion equation,

$$\frac{\partial n(r)}{\partial t} = D \nabla^2 n(r) \quad (2.53)$$

where D is the Effective diffusion coefficient in square meters per second. For a cylindrical column of ionization with initial radius r_0 , Jones (1995) has shown that, provided $4Dt \gg r_0^2$, the appropriate solution of this equation is

$$n(r, t) = \frac{q}{\pi a^2} \exp\left(-\frac{r^2}{a^2}\right) \quad (2.54)$$

where q is the electron line density, and $a^2 = 4Dt + r_0^2$. Jones pointed out that the inequality $4Dt \gg r_0^2$ may not always be satisfied in the early stages of diffusion. This fact, taken together with the non-Gaussian form of the initial distribution, indicates that equation (2.54) should be applied with caution when t is small. The effective diffusion coefficient for electrons in a meteor trail may be written as

$$D = D_i(1 + T_e/T_i) \quad (2.55)$$

where D_i is the diffusion coefficient for positive ions and T_e and T_i are the electron and ion temperatures respectively. The ions and electrons can be considered in thermal equilibrium with the ambient atmosphere except in the very early stages of the formation of a meteor trail, so that T_e can be equated to T_i , and $D = 2D_i$. The diffusion coefficient D_i can be described in terms of the zero field mobility K of a group of ions, using the Einstein relation

$$D_i = kT_iK/e \quad (2.56)$$

where k is Boltzmann's constant and e is the electronic charge. Since K is inversely proportional to the molecular concentration of the ambient gas, D in case of ambipolar diffusion becomes

$$D = 2D_i = 6.390 \times 10^2 KT^2/p = 1.41 \times 10^{-5} T^2/p \quad (2.57)$$

where p is the atmospheric pressure in pascals. It must be taken in account of two cases, the first in which electrons are moving parallel to the magnetic field in the absence of positive ions, then the diffusion coefficient is

$$D_{e\parallel} = kT/m_e\nu \quad (2.58)$$

where ν is the collision frequency and m_e is the electron mass. In the second case, electrons can be moving transverse to the magnetic field, then the diffusion coefficient is written as

$$D_{e\perp} = D_{e\parallel}\nu^2(\nu^2 + \omega^2) \quad (2.59)$$

where ω is the angular gyro-frequency. Only at height of about 95 km the value of $D_{e\parallel}$ becomes equal to D_i and at greater heights becomes much less than the value for the positive ions. For this reason the trails can become elliptical in cross-section. In fact it is known that after formation a meteor trail has a circular cross-section defined by the initial radius and eventually can develop at heights above 95 km an elliptical cross-section like it has been said.

Chapter 3

PRISMA project

What is PRISMA (Prima Rete Italiana per la Sorveglianza sistematica di Meteore e Atmosfera)? It is the first network for systematic surveillance of meteor and atmosphere. This project envisages the creation of an Italian network of all-sky cameras for the observation of fireballs and meteors, in order to determine the objects' orbits and limit the impact areas with a good approximation, in this way facilitating the recovering of eventual fragments. Systematic monitoring of cloud cover and electrical activity will be used for validating meteorological models. In this project there aren't only researchers of different Universities and members of the National Institute of Astrophysics, amateur astronomer, astronomical and meteorological observatory but schools are also involved with a didactic program and with astronomy workshops. PRISMA primary goal is the fireballs monitoring for the recovery of any meteorites with the progressive dislocation of a good number of all-sky automatic cameras throughout Italy, so as to have a camera every 80-100 km. As Italy has an area of 301.338 km^2 , it needs about 50 cameras to cover the whole territory with squares of 80 km of side. Actually, on January 2018 there are 40 all-sky cameras (20 devices in full working mode and 20 in setup phase), but on May 2017 the PRISMA cameras were five only, mostly in northern Italy (fig. 3.1). The PRISMA project is an international European collaboration with the French project FRIPON (Fireball Recovery and InterPlanetary Observation Network), started in 2014 and managed by l'Observatoire de Paris, Muséum National d'Histoire Naturelle, Université Paris-Sud, Université Aix Marseille and CNRS (Colas et al., 2015).



Figure 3.1: The figure shows a map of the PRISMA stations (red working, orange in setup phase and yellow still to buy) and the FRIPON stations (blue)

3.1 Basler Camera

The instrument used in this project is an all-sky camera, in particular a acA1300-30gm Basler ace GigE camera with a Sony ICX445 CCD sensor, figure 3.2.



Figure 3.2: acA1300-30gm Basler Camera

Figure 3.3 shows how a Prisma camera is in general. Usually these cameras are mounted vertically and see all the sky day and night. The images taken from the CCD camera are analyzed in real time by FreeTure, i.e. Free software to capture meteors (Audureau et al., 2015). For meteors capture FreeTure uses the subtraction of two consecutive frames with a detection threshold. In order to decrease false positives, before starting a detection FreeTure waits for a third frame with something that moves in the FOV. Every time something bright passes through the field of view of the camera there is a detection and all the images regarding the event, in standard FITS format, are saved in the HDD of the PC that controls the camera. Subsequently, the images are transmitted through a VPN connection to the FRIPON's server. In this way it is possible to verify if the detection has been done also from other stations and, if so, proceed with the astrometric reduction and computation of the fireball trajectory.

The camera is connected via LAN to a local mini-PC with Linux-Debian operating system and equipped with a mass storage device of about 1 TB. Usually, the camera takes images at a frame rate of 30 per second and only bright fireballs can be imaged. Every 10 minutes a calibration image with an exposure time of 5 s is taken. In these calibration images there are stars up to the apparent mag +3.5 that are used for the astrometric calibration of the camera using a pipeline with the software SExtractor and SCAMP. SExtractor is a program that builds a catalog of objects from an astronomical image, while SCAMP reads SExtractor catalogs and computes astrometric and photometric solutions for any arbitrary sequence of FITS images in a completely automatic way (Bertin and Arnouts, 1996; Bertin, 2006). As astrometric catalog SCAMP uses the Tycho 2 star catalog. For the known stars the accuracy of astrometric calibration is between 100 and 200 arcsec root mean square more frequently around 150 arcsec.



Figure 3.3: Loiano camera PRISMA

3.2 General specifications

The instrument's general specifications has been given by the constructor, they can be read in table 3.1.

Specifications	acA1300-30gm
Resolution H x V Pixels	1296x966
Sensor Type	Sony ICX445AL Progressive scan CCD Global shutter
Optical size	1/3"
Effective Sensor Diagonal	6.1 mm
Pixel Size (HxV)	3.75 μm x 3.75 μm
Frame Rate (at default settings)	30 fps
Mono/Color	Mono
Lens Mount	C-mount, CS-mount
Size (L x W x H)	42.0 mm x 29 mm x 29 mm (without lens mount or connectors) 60.3 mm x 29 mm x 29 mm (with lens mount and connerctors)
Weight	$\leq 90g$

Table 3.1: The table shows the camera specifications

It can also be seen the spectral response of the camera, excluding lens characteristics and light source characteristics, in figure 3.4. In this thesis it is fundamental to know in which band the camera works better. For this purpose some tests are been made on a single Basler camera, property of INAF-OAF (Istituto Nazionale di Astrofisica and Osservatorio di Astrofisica e Scienza dello Spazio of Bologna). The results has been used to calibrate the strumental magnitude obtained through the process of aperture photometry with software Midas.

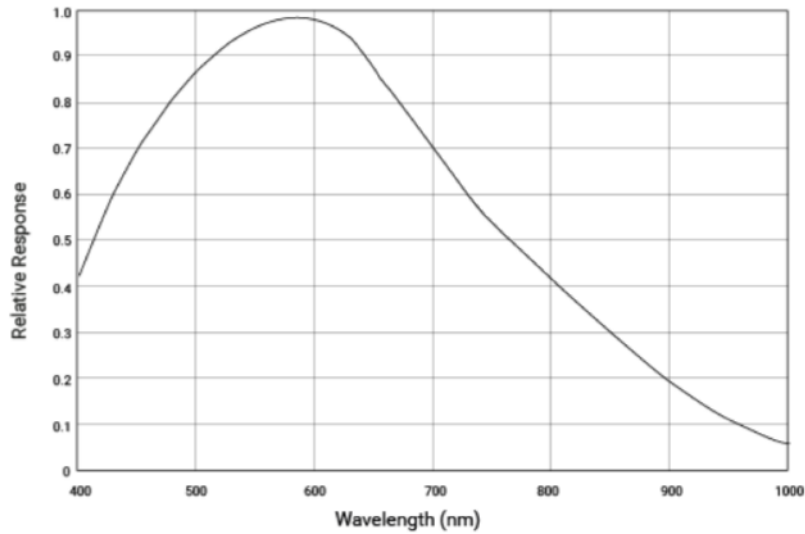


Figure 3.4: The spectral response curve taken from the user manual of Basler camera.

3.3 Stress test Results

The first test, which the camera has been subjected to, consisted in taking 11 dark frames for every different exposure times while the ambient temperature decreased. First it must to be stress that the camera doesn't have a cooling system but it dissipates or absorbs heat from the metal container. The variation of temperature has been measured with a simple ambient thermometer and the camera has been cover with a hood of paper and scotch tape. For this test the camera has been set with gain 400, digital shift, 2 and since the camera can work with 8 bit of sampling or 12 bit, it has been chosen to use 12 bit. The gain and digital shift are settings which is indicated with how many electrons that get converted into a digital number, or electrons per ADU (e^-/ADU). Gain set at 400, it is the maximum while digital shift have an interval from 0 to 4. The exposure times that have been chosen are: 1/10 sec, 1/2 sec, 1 sec, 2 sec, 4 sec, 5 sec and 10 sec. The starting ambient temperature was $24.6^{\circ}C$ while the camera switched on, it had a temperature of $31.5^{\circ}C$. In table 3.2 are listed all the intervals of tempertures which darks has been taken in for every exposure times.

Temperature	Ambient	Camera
1	24.6°C	31.5°C
2	5.8°C	22/20.1°C
3	5.7/5.5°C	17.1/16.7°C
4	-6.6/ - 8.4°C	14/11.3°C
5	-9/ - 11.2°C	9/6.8°C
6	-13.6/ - 14.8°C	4/2.4°C
7	-16/ - 16.6°C	0/ - 1.4°C
8	-17.2/ - 17.6°C	-3/ - 4.5°C
9	-19.2/ - 19.5°C	-11.2°C

Table 3.2: Intervals of Temperatures

Later, every stack of images has been reduced to a masterdark with the software AstroImageJ [11], which means that it has been made the median for all stacks of eleven images. In the end 63 masterdarks has been obtained, which has been used of those only related to exposure times of 1, 2, 4 and 5 sec, because these are the most likely times used for scientific purposes. In figure 3.5, it can be seen the trend of the standard deviations of masterdarks at different exposure times. Moreover, it can also be noted that there is a plateau of a few hundreds on the y axis for every exposures from temperature of 20°C while the temperature is decreasing.

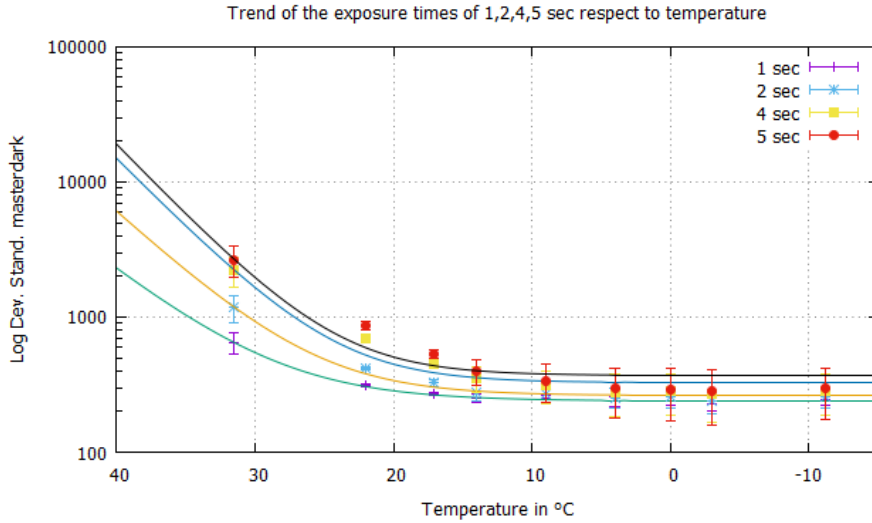


Figure 3.5: Masterdarks related to exposure times of 1, 2, 4 and 5 sec. On y-axis there is the logarithm of standard deviation and on x-axis there's the temperature

This plateau has been reconducted to the presence of a bias, linked to the setting of digital shift. So it has been repeated the process likewise for the dark.

It have been taken 21 frames of bias for every digital shift with exposure time set to $20\mu s$ while the temperature was decreasing. In the following table 3.3 are listed the datas related to the masterbias obtained one more time with the software AstroimageJ, making the median of every stacks of 21 frames.

Temperature	Standard Deviations				
	ds 0	ds 1	ds 2	ds 3	ds 4
$21.5^{\circ}C$	48.677	98.517	198.439	398.410	798.452
$17.1^{\circ}C$	46.845	94.376	190.180	381.005	765.994
$15.6^{\circ}C$	47.913	96.087	193.595	387.905	777.420
$10.7^{\circ}C$	45.795	93.041	187.774	379.153	769.140
$4.6^{\circ}C$	53.311	105.725	204.177	400.657	788.044
$0.8^{\circ}C$	50.359	99.926	201.125	407.036	819.745

Table 3.3: Bias for different digital shift

Plotting the datas it could be noted like the digital shift could influenced the quality of the image. As it can be seen in figure 3.6 changing the value of digital shift the standard deviation of the masterbias has doubled. In the case of Prisma has been useful to do this discovery even if the camera settings could not be change after the installation. Prisma's cameras all work with a digital shift equal to 3, so when an image is taken, it has to be hold in consideration that it will have a bias equal to standard deviation 400.

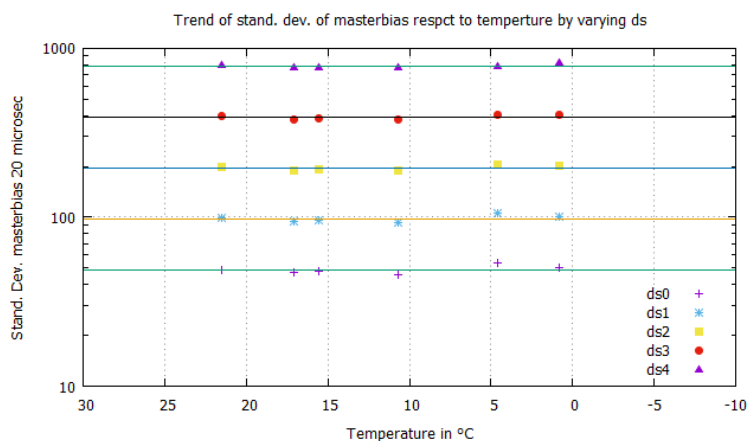


Figure 3.6: Masterbias related to exposure times of 1, 2, 4 and 5 sec. On y-axis there is the logarithm of standard deviation and on x-axis there's the temperature

In conclusion, after having been taken these tests, it could be said that an eventual cooling system could be implemented to the camera but the advantages won't be comparable to the expense.

3.4 Photometric characterization

Like it has been said, it has been fundamental understanding which photometric band the camera works in. For these purpose images of Perseids' shower have been used, working with the software Midas. First of all, these images have been taken in the night of 12 August 2017 at a temperature of 20°C , with settings of the camera as exposure time of 4 seconds, mode 12 bit, gain 400 and digital shift 3. Before using Midas to perform aperture photometry, the images has been reduced with a masterdark and a masterbias, using the software AstroImageJ. This operation has allowed to eliminate a good portion of bad pixels. The following figure 3.7 is an example of one of the reduced images used for the aperture photometry.

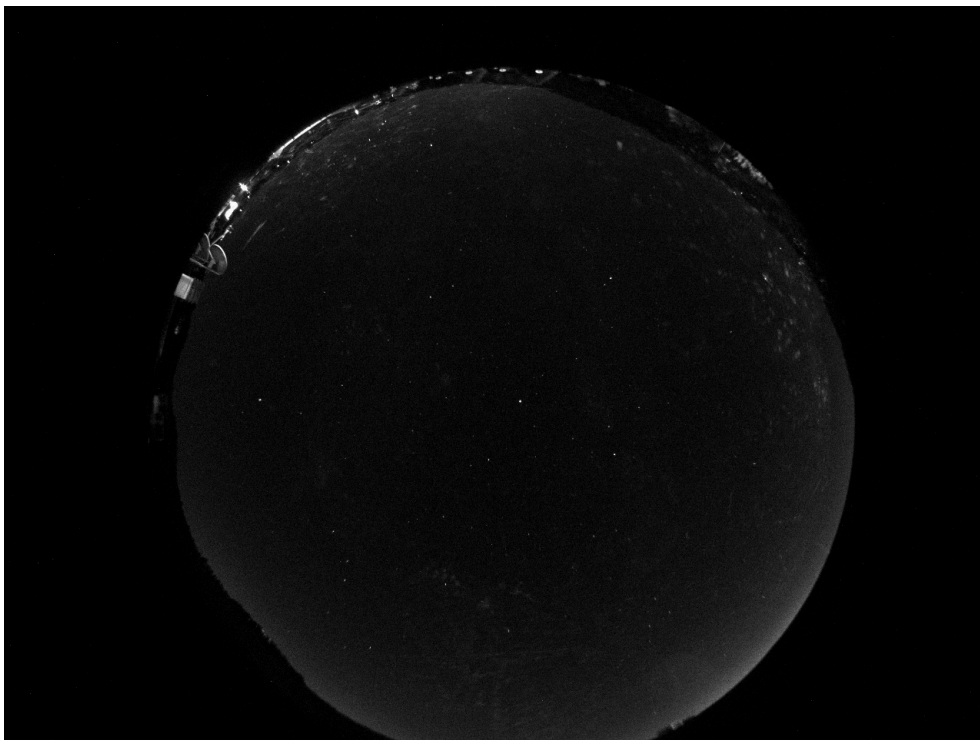


Figure 3.7: This figure shows an image of Perseids' shower of 12 August 2017 taken from the station of Bologna. It cannot be seen the shower in this image because it has been chosen to perform the photometry only on stellar images, without meteoric phenomena.

After the cleaning of the images, four images has been chosen for the photometry. Aperture photometry consists in measuring the flux of a source within an area, called aperture, and it is applied for field of view not too crowded like in this case. So every single image has been opened with the software Midas [10]. The ESO-MIDAS system provides general tools for image processing and data reduction with emphasis on astronomical applications, in addition it contains applications packages for stellar and surface photometry, image sharpening and decomposition, statistics and various others. To do aperture photometry, the following commands have been executed:

1. inmidas (enter midas)
2. crea/disp 0 680,460 (create a display)
3. load/lut rainbow (load a look up table)
4. load/itt log (modify the lut)
5. disp/lut (display the lut)
6. load/ima "nome.fits" center=C,C scale= \pm ? cuts=0,80000 (load the image with some parameters)
7. mag/circle ? ? target,noman's land, sky (execute aperture photometry)

Before this process has been executed for all four images, about twenty stars have been identified with the eye and the help of a sky chart taken from the site Heavens Above [12], in every image, see table 3.4. Aperture photometry has been made on these stars obtaining a list of parameters like position on the image (x,y), counts, flux, sigma and instrumental magnitude.

Name	RA	DEC	Spectral Type	B	V	R	I
Vega	18 36 56.33635	+38 47 01.2802	A0Va	0.03	0.03	0.07	0.10
γ Lyr	18 58 56.62241	+32 41 22.4003	B9III C	3.20	3.25	3.27	3.28
β Lyr	18 50 04.79525	+33 21 45.6100	B8.5Ib-II C	3.42	3.42	3.31	3.29
Deneb	20 41 25.91514	+45 16 49.2197	A2Ia C	1.34	1.25	1.14	1.04
δ Cyg	19 44 58.47854	+45 07 50.9161	A0IV C	2.85	2.87	2.88	2.90
γ Cyg	20 22 13.70184	+40 15 24.0450	F8Ib C	2.90	2.23	1.74	1.40
π Her	17 15 02.83436	+36 48 32.9843	K3III C	4.61	3.18	2.22	1.49
η Her	16 42 53.76509	+38 55 20.1129	G7IIIFE-1 C	4.42	3.50	2.38	2.35
ξ Her	17 57 45.88571	+29 14 52.3675	G8.5III B	4.64	3.70	3.01	2.55
Altair	19 50 46.99855	+08 52 02.9563	A7Vn	0.98	0.76	0.62	0.49
γ Aqr	19 46 15.58029	+10 36 47.7408	K3II B	4.23	2.72	1.65	0.87
β Dra	17 30 25.96170	+52 18 04.9993	G2Ib-IIa B	3.79	2.81	2.12	1.64
Arturo	14 15 39.67207	+19 10 56.6730	K1.5IIIFe-0.5B	1.18	-0.05	-1.03	-1.68
β Boo	15 01 56.76238	+40 23 26.0406	G8IIIaFe-0.5 C	4.47	3.52	2.85	2.37
γ Boo	14 32 04.67180	+38 18 29.7043	A7IV+(n) C	3.21	3.02	2.88	2.80
δ Boo	15 15 30.16295	+33 18 53.3926	G8IIIFe-1 B	4.44	3.49	2.76	2.25
ρ Boo	14 31 49.78962	+30 22 17.1781	K3-III B	4.89	3.59	2.67	2.02
η Uma	13 47 32.43776	+49 18 47.7602	B3V B	1.67	1.86	1.98	2.16
ϵ Uma	12 54 01.74959	+55 57 35.3627	A1III-IVpkB9	1.75	1.77	1.79	1.82
α Oph	17 34 56.06945	+12 33 36.1346	A5III C	2.22	2.07	1.93	1.85

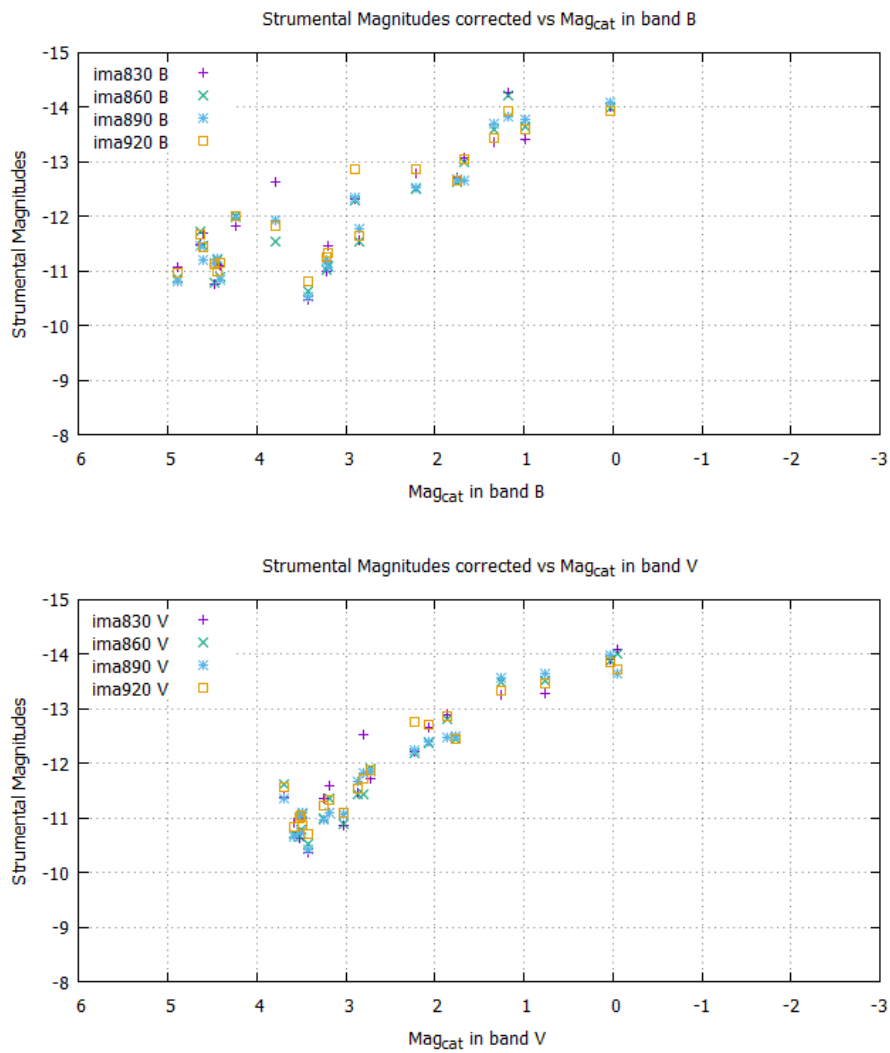
Table 3.4: List of identified stars in every image

Strumetal magnitudes have been corrected in each band for the airmass, that has been calculated, finding the elevation with another software, called Heavensat [13].

$$Airmass = \frac{1}{\cos(\alpha)} \text{ where } \alpha = 90^\circ - \text{Elevation} \quad (3.1)$$

$$\text{Strum.Mag. corrected} = \text{Strum.Mag.} - (\text{Airmass} * \text{coeff.band}) \quad (3.2)$$

where coeff.band was 0.20 in B, 0.10 in V, 0.08 in R and 0.06 in I, correction factor for the site of Loiano. Then the corrected strumetal magnitudes have been plotted versus catalog magnitudes (fig.3.8), taken from an online catalog, Simbad.



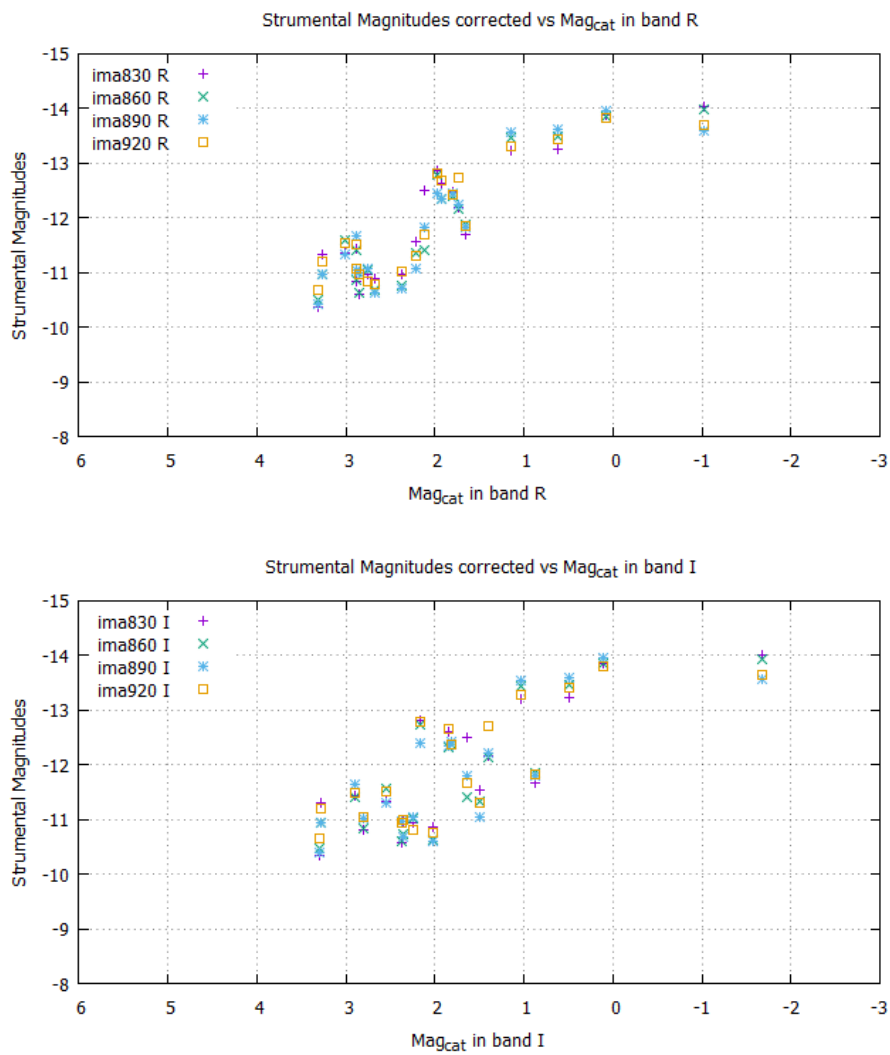
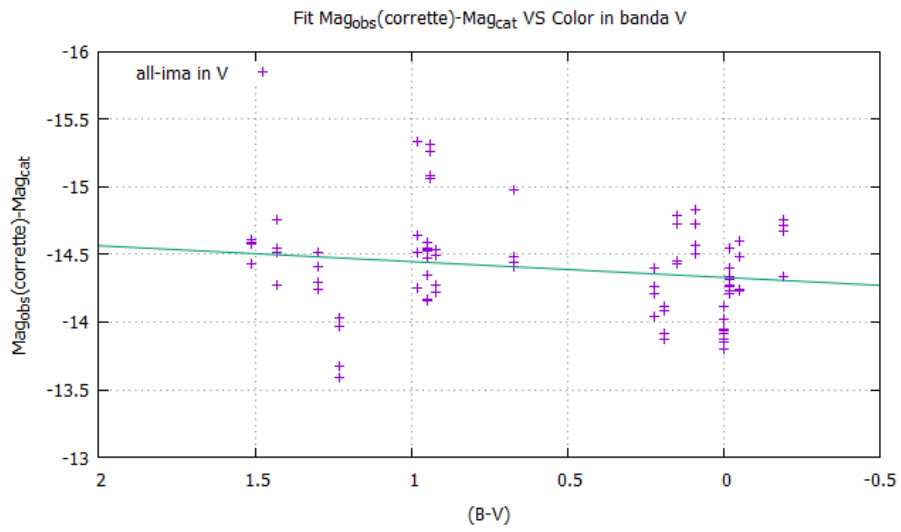
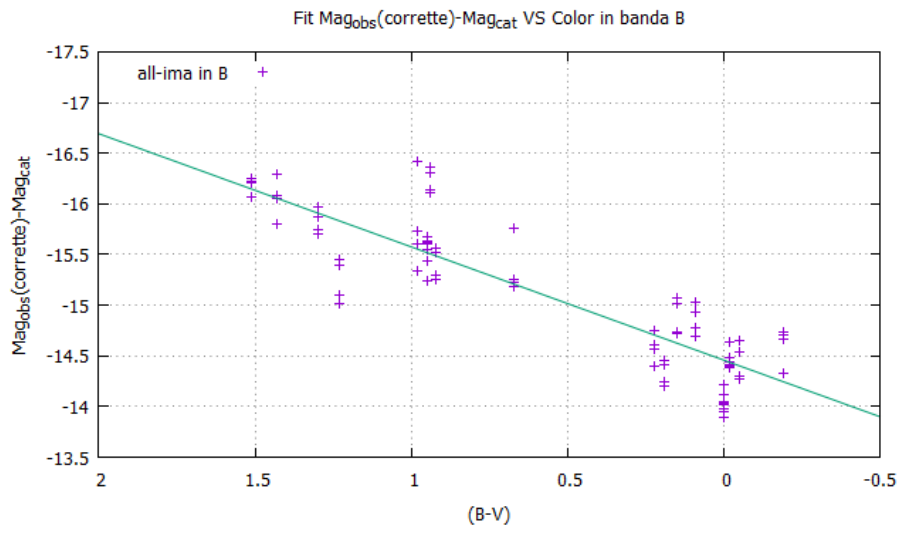


Figure 3.8: Strumetal magnitudes vs Catalog magnitudes in band B,V,R,I

Now to understand which band the camera works in, the difference between strumetal magnitudes and catalog magnitudes has been plotted vs the color associated to the band, fitting the datas like in figure 3.9.



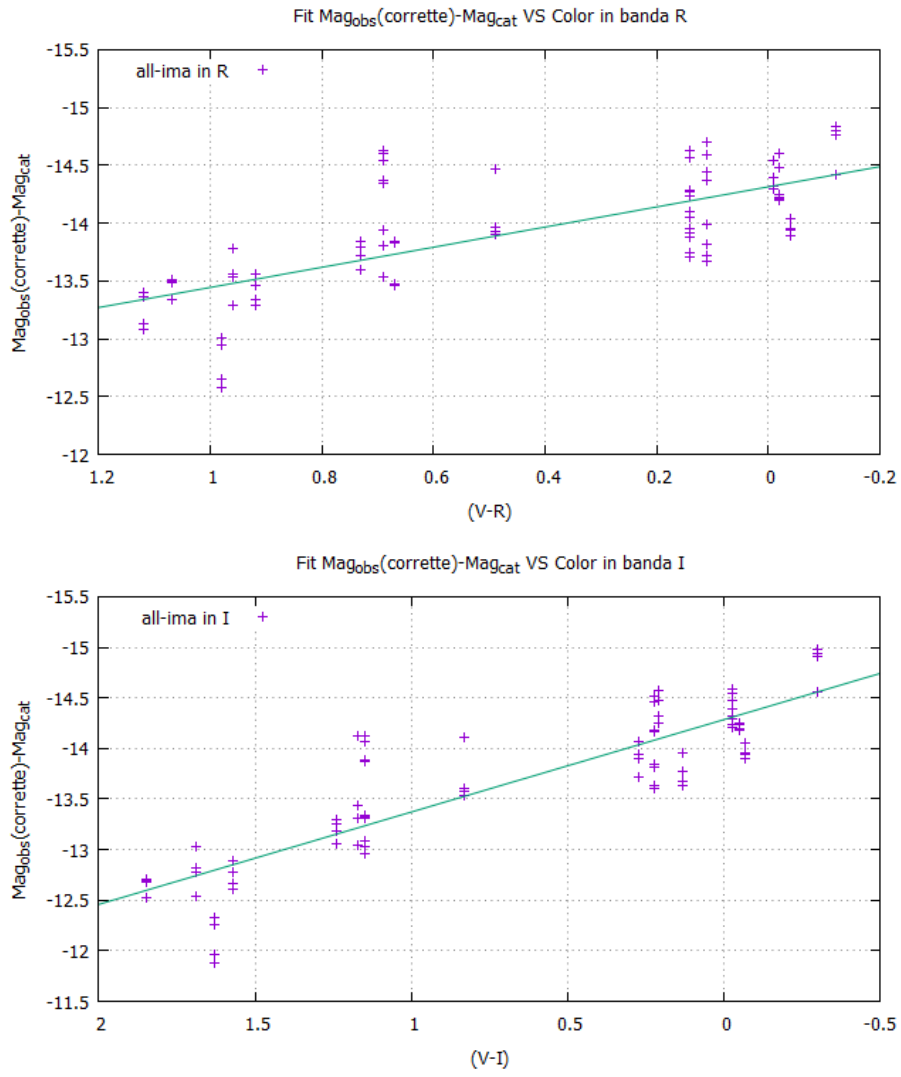


Figure 3.9: ΔMag_{oss} vs $Color_{cat}$ in band B,V,R,I

The datas for each band have been plotted with a fit of this form:

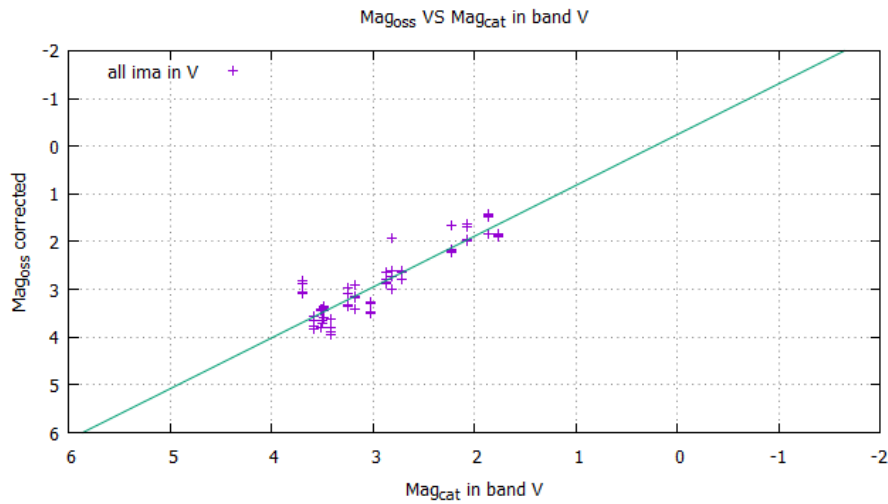
$$mag_{oss} - mag_{cat} = k (color) + w \quad (3.3)$$

In this way it was possible to obtain the coefficients k and w , where respectively k is color term that indicates how wrong the strumental magnitudes are respect to those from catalog and w is the offset. The aforementioned figure shows how the camera seems to respond better in band V respect to the other band, whose the coefficients k are not approximated to zero (see table 3.5).

	k	w
Band B	-1.11687	-14.4579
Band V	-0.117308	-14.3302
Band R	0.869979	-14.3137
Band I	0.913123	-14.2843

Table 3.5: Coefficients k and w of the four fit in different band from fig 3.9

At this point, the magnitudes observed have been corrected for the color term and the offset, furthermore the stars saturated have been removed one at time. In this way every time a star saturated has been removed from the fit, the root mean square, rms, decreased. The final result can be seen in figure 3.10 for each band.



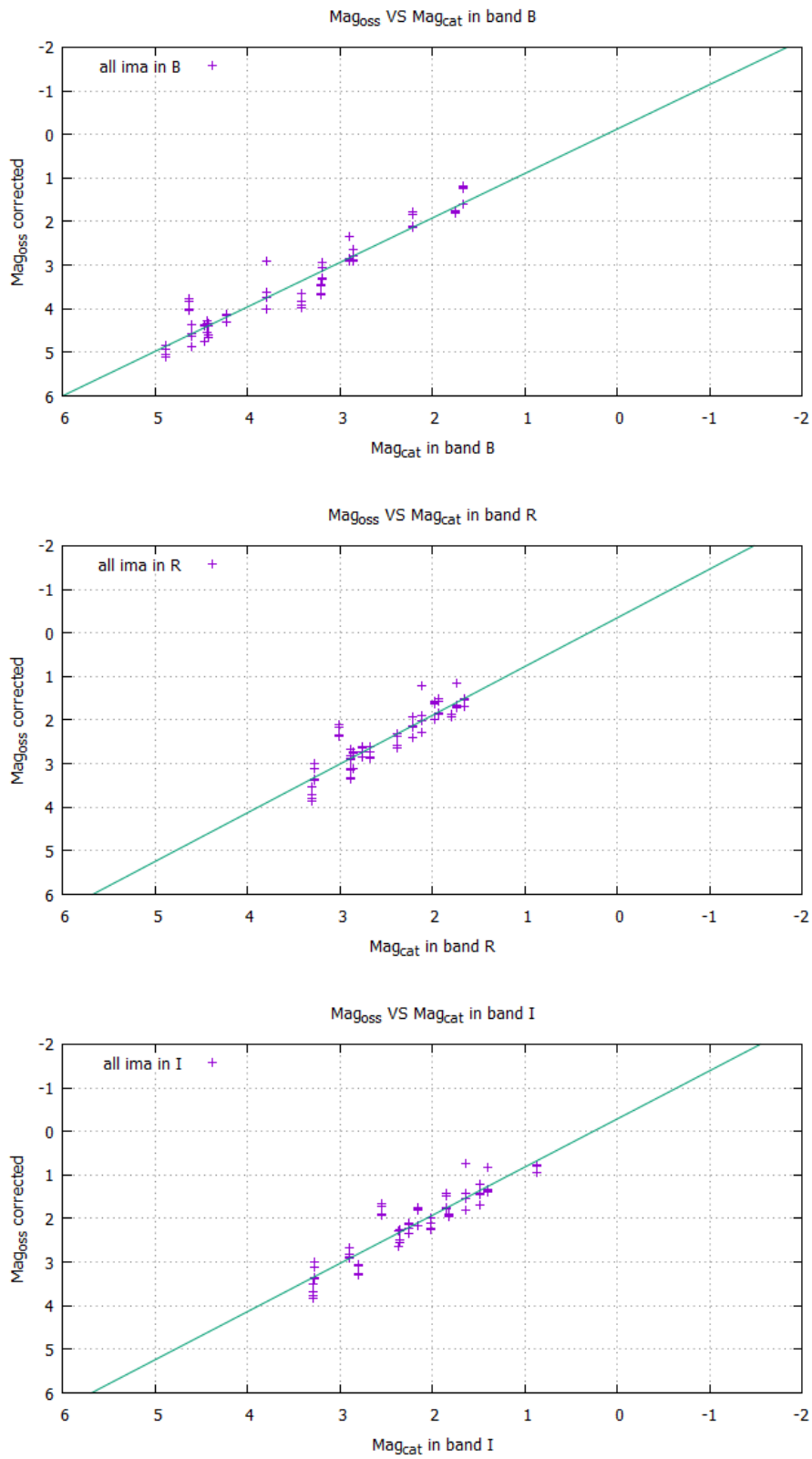


Figure 3.10: Mag_{oss} vs Mag_{cat} in band B,V,R,I

In detail, in figure 3.11 it can be seen how the rms has changed for every star eliminated from the fit.

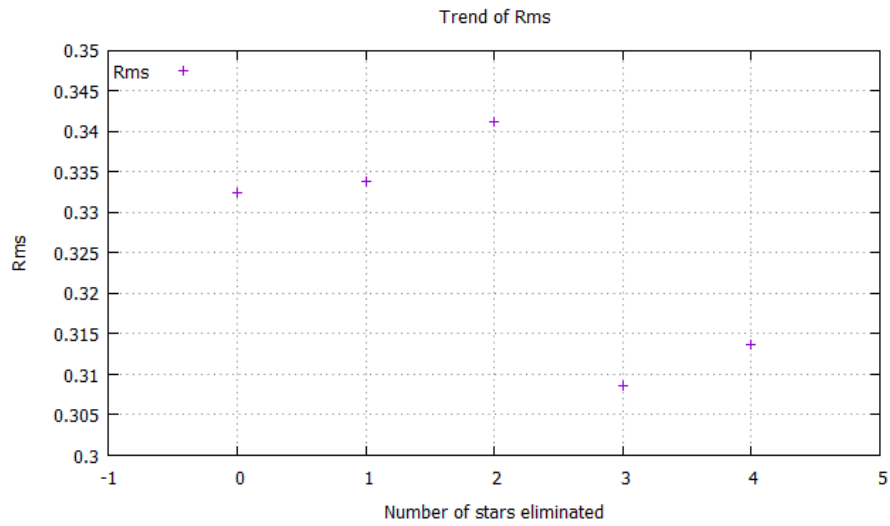


Figure 3.11: Example of trend of rms in band B

Chapter 4

Astrometric characterization of PRISMA cameras

When an event, like a bolide, happens Prisma's cameras records the event with specific settings. Before the camera have others settings to take calibration images. In the specific, the settings for the calibration images are:

- First of all these images are taken before and after the event every 10 minutes;
- The exposure time is set to 5 seconds;
- The gain is set to 400.

In this way every night about an hundred of images are taken, which is important because having several images that cover a period from few nights to even six months, allows to arrive at an astrometric solution that will be applied to the event's images. Instead, when a camera senses an events, it becomes to take the images with others settings, in particular the exposure time changes to 1/30 seconds, leaving the same others parameters.

4.1 Cleaning of the images

Before beginning the astrometric process it is necessary to clean the calibration images from bad pixels. To do this, it is needed to create a sort of a masterdark. So a median is created from some of the calibration images with the program AstroImageJ. After that, this Dark median is applied at all of the calibration images. The figures 4.1 and 4.2 show an example of cleaning with the pseudo dark median.

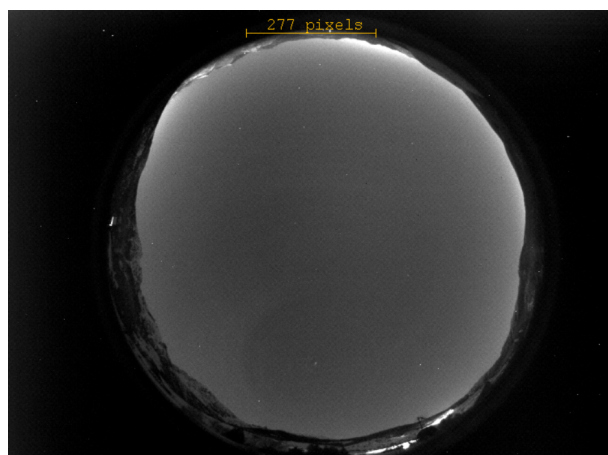


Figure 4.1: This figure shows the pseudo dark median.

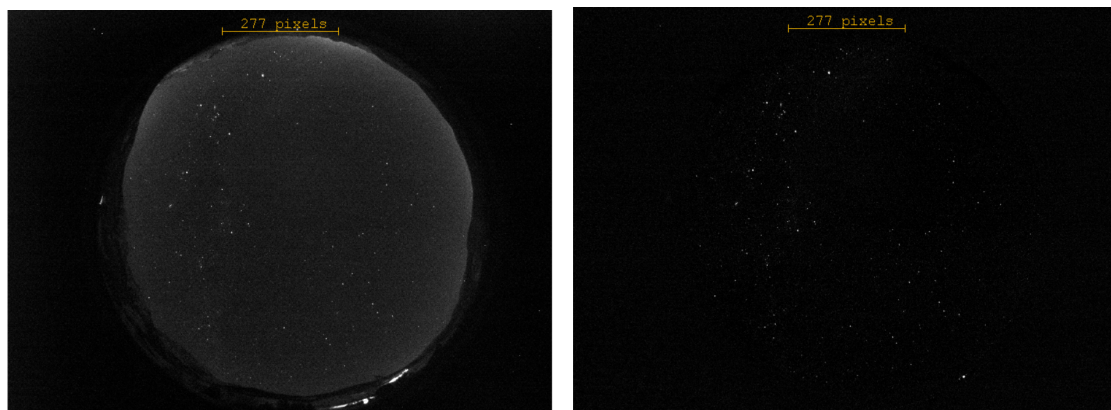


Figure 4.2: To the left it can be seen an example of a raw calibration image, to the right an example of a cleaned calibration image taken with the PRISMA camera of Lignan.

4.2 Astrometric Pipeline

As said, after cleaning, the calibration images are processed to find a global astrometric solution that it will be applied at the event images. Doing this, it is possible to discover the wcs (world coordinate system) coordinate of the meteoroid. The astrometric pipeline consists in the use of two softwares SExtractor (Source Extractor) and Scamp. In the specific the first software it is used to obtain for each calibration image a catalog of stars that appear on the field. While the second software is used to match the obtained catalogs with an existing star catalog, in this case Tycho-2, so obtaining an astrometric solution to be applied at the event images.

4.2.1 SExtractor (Source Extractor)

SExtractor is the first software used in the astrometric process. This software works in steps. The first step consists in determining the background and if pixels belong to background or objects. Then it splits up the area that is not background into separate objects and determines the properties of each detected object, and so writing a catalog for each image. All the pixels above a certain threshold are taken to belong to an object. And if, for example, there is a saddle point in the intensity distribution, the object is split in different entries in the output catalog. Photometry is done on these by dividing up the intensity of the shared pixels. Moreover there is the possibility to "clean" the catalog in order to eliminate artifacts caused by bright objects (like saturated objects). Just as said, it is obtained a catalog of classified objects like stars and galaxies by a neural network.

All these steps are obviously controlled by a series of parameters/keywords (described in the following sections). Also, in input SExtractor can read weight maps and it can give as output fits files to check how and what is extracted, the check images.

Summing up, the steps, that SExtractor does, are:

1. Measure the background and its RMS noise (background and RMS maps)
2. Subtract background
3. Filter (convolve with specified profile)
4. Find objects (thresholding)
5. Deblend detections (break up detection into different objects)
6. Measure shapes and positions

7. Clean (reconsider detections, accounting for contributions from neighbors)
8. Perform photometry
9. Classify the detections as star or galaxy
10. Write an output catalog and eventual check images

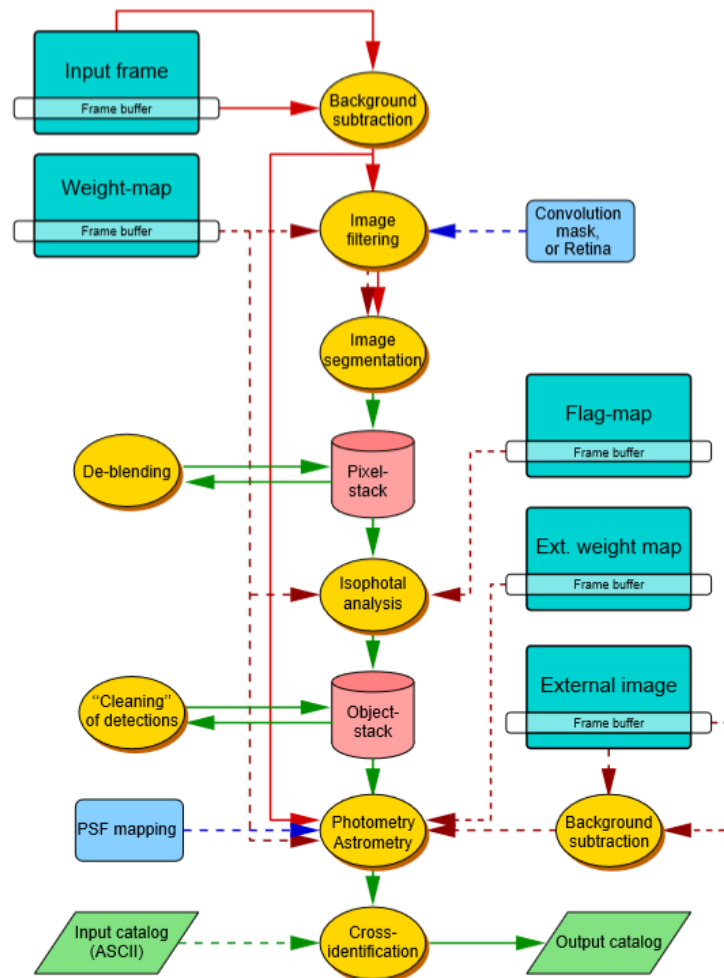


Figure 4.3: This figure shows a diagram taken from the manual of SExtractor explaining all the main steps and also the many extra options over a simple run of SE.

Configuration file: default.sex

SExtractor can be used in three ways: on a single image (like in this work) for both detection and photometry, on two images, one for detection and the other for photometry and on two images with cross-identification in the catalogs. SExtractor needs a series of parameters in order to run. These parameters can be given at the command line or in a configuration file. The command line to run SExtractor is:

```
sextractor image -c configuration-file.txt
```

If sextractor doesn't find a configuration-file.txt, then it will try to read "default.sex" from the local directory. In the following pages can be seen an example of configuration file, used in this work. This file is very useful way of remembering which parameters it has been used in running SExtractor and there is no need to reset all parameters when running SExtractor over a series of files. The configuration file is an ASCII file with the name of the parameters and the value on separate lines. A comment line begins with "# " and ends with the end-of-line. Following the divisions of the configuration file, it will be discussed in the next paragraphs every single keyword.

Catalog parameters

The first parameters in the configuration file refers to the output catalog. The parameter CATALOG-NAME is the name of the output catalog that can be chosen. Next it can be chosen the extension of the catalog. In this work it is used FITS-LDAC because, as it will be explained later, the second software, Scamp, asks for a binary catalog in input. The last parameter in this part is PARAMETERS-NAME, this is a file ASCII which there are listed in a series of parameters that will be calculated and written in the output catalog. Further on, it will be explained in detail what is a parameter file.

Extraction parameters

The second set of parameters are information on the image and how the extraction of the objects must be done. SExtractor gets the positional information from the FITS header but most of the following parameters must be specified. The DETECT-TYPE specifies what type of data the software is handling, scanned photo plates or CCD data.

Thresholding is mostly controlled through the DETECT-MINAREA, DETECT-MAXAREA and DETECT-THRESH. DETECT-MINAREA and DETECT-MAXAREA

allow to set the minimum number of pixels a group should have to trigger a detection, on the other hand, the other sets the maximum number of pixels a group must have in order to trigger a detection. While DETECT-THRESH sets the threshold value. They can be used to type of threshold RELATIVE, i.e., in units of sigma and ABSOLUTE, i.e., in units of ADU's or Surface Brightness (4.1).

$$threshold = 10^{-\frac{SB_{limit} - SB_{zeropoint}}{2.5}} \quad (4.1)$$

If one single value is given, it is interpreted as a threshold in units of the background's standard deviation. Then ANALYSIS-THRESH is just the threshold for CLASS STAR and FWHM, all other paramter are determined from the DETECT-THRESH. It can be also applied a filter the keyword are FILTER and FILTER-NAME, this filter essentially smooths the image. FILTER allow you to decide if apply o not a filter with a YES or NO. FILTER-NAME allows you to choose what filter to apply. There are four type of filters in sextractor directory: Gaussian, Mexican hat, Tophat and blokfunction of varius sizes, all normalized. In detail:

1. default.conv is a small pyramidal function and it is fast.
2. gauss.conv can be found in different functions, for seeing FWHMs between 1.5 and 5 pixels (best for faint object detection).
3. tophat.conv is a set of top-hat functions. Use them to detect extended, low surface brightness objects, with a very low threshold.
4. mexhat.conv is a wavelets, producing a passband-filtering of the image, tuned to seeing FWHM's between 1.5 and 5 pixels. it is useful in very crowded star fields, it may need a high threshold.
5. block-3x3.conv is a small block function (for rebinned images)

The next step is deblending which is the part of SExtractor where a decision is made whether or not a group of adjacent pixels above threshold is a single object or not. The parameter DEBLEND-NTHRESH helps to separate near objects with both pixels above threshold. First sextractor defines a number of levels between the threshold and the maximum count in the object. This is set by the DEBLEND-NTHRESH parameter. The levels are spaced exponentially. SExtractor then constructs a tree of the objects, branching every time there are pixels above a threshold separated by pixels below it, see in figure 4.4. A branch is considered a different object provided that the number of counts in the branch (A in the figure) is above a certain fraction of the total count in the entire island. And moreover there is at least one other branch (B in the figure) above the same level that is also above this fraction. This fraction is defined in DEBLEND-MINCONT.

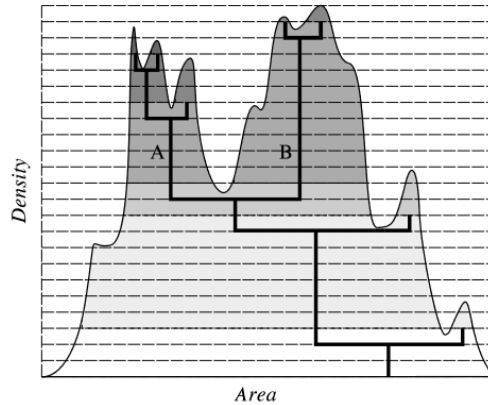


Figure 4.4: An illustration of how works DEBLEND-NTHRESH and DEBLEND-MINCONT

There is also the option to clean the list of objects of artifacts due to bright objects. So, this can be set CLEAN to YES. All the detections are checked to see if they would have been detected if their neighbors were not there. To do this, the contributions of the neighboring objects has to be computed. an estimate is made from a moffat light profile. The Moffat profile is scaled and stretched to fit the neighbour's profile. The contribution to the object from the wings of the Moffat profile is then subtracted. The Moffat profile is written as

$$\frac{I(r)}{I(0)} = \frac{1}{(1 + kxr^2)^\beta} \quad (4.2)$$

In formula 4.2 the CLEAN-PARAM is the β parameter. So decreasing CLEAN-PARAM yields brighter wings and more aggressive cleaning. This value goes from 0.1 to 10.

Weighting parameters

Sextractor is able to handle images with variable noise. It does it through weight maps, which are frames having the same size as the images where objects are detected or measured, and which describe the noise intensity at each pixel. Different option are available: the background as determined by the software or an external weight image. If an external weight map is given, it has to be specified what kind it is; a variance map or a rms map or a weight map, from which a variance map should be derived. The weight for each pixel is derived as follows:

$$weight = \frac{1}{variance} = \frac{1}{rms^2} \quad (4.3)$$

With the keyword WEIGHT-TYPE it can be chosen different types of weight-maps, these can either be read from a FITS file, whose name is specified by the WEIGHT-IMAGE keyword, or computed internally. Valid WEIGHT-TYPEs are:

- NONE: No weighting is applied. The related WEIGHT-IMAGE parameter is ignored.
- BACKGROUND: the science image itself is used to compute internally a variance map (the relate WEIGHT-IMAGE is ignored). Robust (3σ -clipped) variance estimates are first computed within the same background meshes. The resulting low-resolution variance map is then bicubic-spline-interpolated on the fly to produce the actual full-size variance map.
- MAP-RMS: the FITS image specified by the WEIGHT-IMAGE file name contain a weight-map in units of absolute standard deviations (in ADU's per pixel).
- MAP-VAR: the FITS image specified by the WEIGHT-IMAGE file name must contain a weight-map in units of relative variance. A robust scaling to the appropriate absolute level is then performed by comparing this variance map to an internal, low-resolution, absolute variance map built from the science image itself.
- MAP-WEIGHT: the FITS image specified by the WEIGHT-IMAGE file name must contain a weight-map in units of relative weights. The data are converted to variance units (by definition variance $\propto 1/\text{weight}$), and scaled as for MAP-VAR. MAP-WEIGHT is the most commonly used type of weight-map: a flat-field, for example, is generally a good approximation to a perfect weight-map.

In this work, it has been used a type of weight map like MAP-WEIGHT. This map has been creating with the software Gimp. First, it has been opened a calibration image with Gimp. Then with the tool Elliptic, it has been designed a frame in a shape of an ellipse (possibly cutting the edges if there are spurious luminous objects and the landscape). After the image has been edited, in the center it has been filled with FG color while in the outwards with BG color. It has been changed the image mode into 2 colors. And finally it has been exported like a mask.fit. In the following figure 4.5 is shown a mask created with this process.

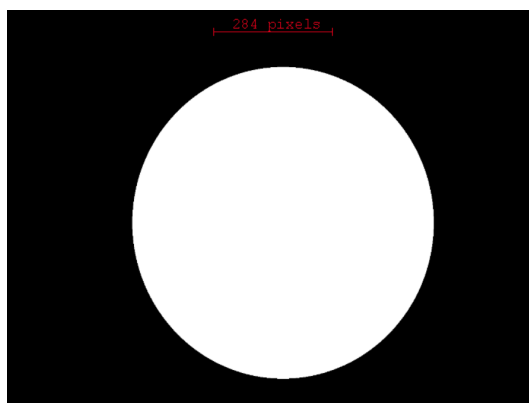


Figure 4.5: The figure shows an example of mask applied through SExtractor to the images.

Flagging parameters

A set of both internal and external flags is accessible for each object. Internal flags are produced by the various detection and measurement processes within SExtractor; they tell for instance if an object is saturated or has been truncated at the edge of the image. External flags come from "flag-map": these are images with the same size as the one where objects are detected, where integer numbers can be used to flag some pixels (for instance, 'bad' or noisy pixels). Different combinations of flags can be applied within the isophotal area that defines each object, to produce a unique value that will be written to the catalog.

The internal flags are always computed. They are accessible through the FLAGS catalog parameter, which is a short integer. FLAGS contains, coded in decimal, all the extraction flags as a sum of powers of 2:

- 1 The object has neighbours, bright and close enough to significantly bias the MAG-AUTO photometry, or bad pixels (more than 10% of the integrated area affected);
- 2 The object was originally blended with another one;
- 4 At least one pixel of the object is saturated (or very close to);
- 8 The object is truncated (too close to an image boundary);
- 16 Object's aperture data are incomplete or corrupted;
- 32 Object's isophotal data are incomplete or corrupted;

64 A memory overflow occurred during deblending;

128 A memory overflow occurred during extraction.

SExtractor understands that it must process external flags when IMAFLAGS-ISO or NIMAFLAGS-ISO are present in the catalog parameter file. It then looks for a FITS image specified by the FLAG-IMAGE keyword in the configuration file. The FITS image must contain the flag-map, in the form of a 2-dimensional array of 8, 16 or 32 bits integers. It must have the same size as the image used for detection. The flag-map values for pixels that coincide with the isophotal area of a given detected object are then combined, and stored in the catalog as the long integer IMAFLAGS-ISO. Five kinds of combination can be selected using the FLAG-TYPE configuration keyword:

- OR: the result is an arithmetic (bit-to-bit) OR of the flag-map pixels.
- AND: the result is an arithmetic (bit-to-bit) AND of non-zero flag-map pixels.
- MIN: the result is the minimum of the (signed) flag-map pixels.
- MAX: the result is the maximum of the (signed) flag-map pixels.
- MOST: the result is the most frequent non-zero flag-map pixel-value.

Photometry parameters

After the cleaning of the image, SExtractor performs astrometry, photometry and finds geometric parameters. The photometry has a few input parameters associated with it. There are five different approaches in SExtractor's photometry: isophotal, isophotal-corrected, automatic, best estimate and aperture.

ISO As it has been said above, a threshold has been set which SExtractor should do at its photometry, with the estimated background as zeropoint. The pixels above this threshold constitute an isophotal area. The flux or magnitude determined from this (counts in pixels above threshold minus the background) is the isophot flux/magnitude. Apart from the threshold (DETECT-THRESH) and the background estimation, there is nothing to influence here.

ISOCOR Normally objects rarely have all their flux within neat boundaries, some of the flux is in the wings of the profile. SExtractor can do a crude correction for that, assuming a symmetric gaussian profile for the object. This would be the isophot-corrected flux/magnitude. There is no parameter to influence this estimate.

AUTO This approach is what has been used in this work. SExtractor uses a flexible elliptical aperture around every detected object and measures all the flux inside that. There are two parameters regulating the elliptical apertures: PHOT-AUTOPARAMS and PHOT-AUTOAPERS. The characteristic radius for the ellipse is:

$$r_1 = \frac{\sum_r I(r)}{\sum I(r)} \quad (4.4)$$

Also known as the Kron radius. From the object's second order moments, the ellipticity η and position angle θ are computed. The major and minor axes of the elliptical aperture are computed to be kr_1/ϵ and r_1 respectively. PHOT-AUTOPARAMS influences directly the estimation. The first is the k factor mentioned above and the second is the minimum radius for a Kron ellipse. PHOT-AUTOAPERS are the minimum aperture diameters for the Kron photometry, estimation and measurement. These are used in case the radius of the Kron aperture goes below the R_{min} specified in PHOT-AUTOPARAMS. The values in the default.sex are probably best for most applications. A good way to check the setting on PHOT-AUTOPARAMS is to generate an APERTURE check-image and see if the Kron apertures overlap too much with those of neighboring objects (see the next sections for an explanation about check-image).

BEST In case photometry could be influenced by nearby sources, it is recommended to use this option. This is usually equal to AUTO photometry but if the contribution of other sources exceeds 10%, it is ISOCOR. That's said AUTO and ISOCOR are at least more consistent.

Another important keyword is PHOT-APERTURES. The apertures are specified in pixels in this keyword. The fluxes, magnitudes and errors in these are specified in FLUX-APER, MAG-APER, FLUXERR-APER and MAGERR-APER (see Output SExtractor paragraph). One of the geometric output-parameters is the half-light radius. The fraction of total light within this radius is specified in the PHOT-FLUXFRAC parameter.

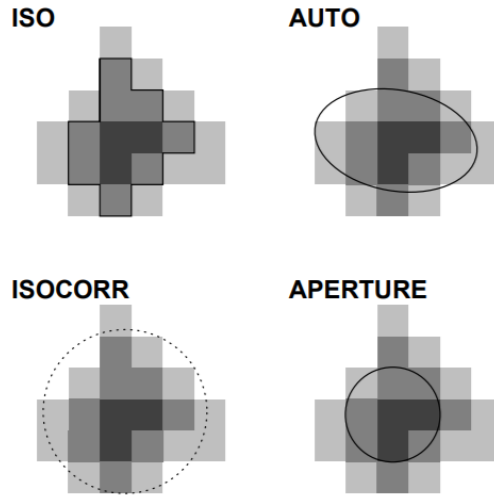


Figure 4.6: The figure shows an example of the four apertures that SExtractor can applied in the process of photometry.

The following keywords as SATUR-LEVEL, SATUR-KEY, MAG-ZEROPOINT, MAG-GAMMA, GAIN, GRAIN-KEY and PIXEL-SCALE are the last parameters to influence the photometry. SATUR-LEVEL is the limit for SExtractor to start extrapolating to get the photometry. The saturation level can be read in the header fits using the keyword SATUR-KEY set to the corresponding keyword, usually SATURATE, into the header. Or it can be given in ADUs with SATUR-LEVEL, in this case it has been chosen to use the last option setting the saturation level to 60000. Next parameter MAG-ZEROPOINT is the zeropoint for the photometric measurements. While MAG-GAMMA is a keyword used when DETECT-TYPE is set to PHOTO mode. GAIN is the ratio of the number of electrons to the number of ADU. The GAIN is dependent on the type of CCD that is used and the instrument in front of it. In this work the GAIN is not specified because it has been used the keyword GAIN-KEY that read the gain value directly into the header fits. Recalling, in PRISMA camera the CCD has a GAIN of 400. These last parameters are used to convert counts to flux and for the calibration of the magnitude scale. The last but not the least is the parameter PIXEL-SCALE that has to be set because SExtractor needs it only for the CLASS-STAR parameter.

Star/Galaxy Separation parameters

The SEEING-FWHM is important for the separation between stars and galaxies. Like PIXEL-SCALE it is only used for the CLASS-STAR parameter if set in default.param. STARNNW-NAME set the name of the file containing the neural

network weights for star/galaxy separation. This file is in the same directory as the other configuration files and it is called `default.nnw`. It is advised not to edit this file.

Background parameters

SExtractor estimates the background of the image as well as the RMS noise in that background, mapping both. It subtracts the estimated background from the photometry and uses the RMS to estimate errors. So the background is important in the rest of the SExtractor run.

`BACK-TYPE` set to `AUTO` allows the software to subtract the background estimated from the image. `BACK-SIZE` regulates the estimate. In an area of the `BACK-SIZE`, the mean and the σ of the distribution of pixel values is computed. Then the most deviant values are discarded and median and standard deviation σ are computed again. This is repeated until all the remaining pixel values are within mean $\pm 3\sigma$. If σ dropped with less than 20% per iteration, the field is considered not crowded. The value for the background in the area is:

1. the mean in the non-crowded case
2. the mode in the other case:

$$mode = 2.5 \times median - 1.5 \times mean \text{ in the crowded case} \quad (4.5)$$

Both the mean and the median are the ones computed in the last iteration. The mean is the average and the median is the average of all the values except the most extreme one. The background map is a bi-cubic-spline interpolation over all the area's of size `BACK-SIZE`, after filtering. So obviously, the choice of `BACK-SIZE` is very important, too small and the background estimate will be partly object flux, too large and small scale variations cannot be taken into account.

Before the fit to the background values is done, the values can be smoothed: `BACK-FILTERSIZE` is the median filter for the background map. Effectively, it smooths the background image over this number of meshes to get rid of the deviations resulting from bright or extended objects.

Check image parameters

To check if SExtractor is doing a good job (as in fig 4.7), there is the option to have as output a series of images in fits. The names for the output fits files are specified in CHECKIMAGE-NAME. It can be given a list of sixteen images, separated by a comma. Meanwhile the type of output wanted is defined in CHECKIMAGE-TYPE. In this word the check images used are OBJECTS and APERTURES. The first is useful to see what SExtractor has extracted, while the second is good diagnostic on whether or not the given threshold is right.



Figure 4.7: This is an example of check image of the extraction of stars from a calibration image of Lignan station. It can be observed how and what sextractor has extracted as objects. In particular the points darker are the objects extracted, the points like at the right bottom are artificial objects while the puntiform points fainter are the bad pixel.

Memory parameters

In this section of the configuration file there are the parameters regulating the memory use of SExtractor. In this case, it is best to keep the default values.

Association parameters

Association parameters are those dealing with crosscorrolating two catalogs: a catalog of targets and the ouput catalog. The cross correlation is controlled by two parameter: ASSOC-RADIUS and ASSOC-TYPE, the first governing the search

radius and latter which objects gets selected if there are multiple candidates near the positions. The numbers of the columns in target catalog which contain the x,y positions of the objects need to be in ASSOC-PARAMS. A third column can be used as weight. This process is useful if one are crosscorellating between catalogs of different filters. Some of the columns in target catalog can be put into the second output catalog. These columns are specified in ASSOC-DATA and end up in the VECTOR-ASSOC. In this work it hasn't been utilized this process because it works only with pixel positions (not RA and DEC).

Miscellaneous parameters

In the last sections they can be find the parameters for the comments. Like VERBOSE-TYPE is the paramter that regulates the amount of comments printed on the command line. It can be put QUIET when for example Sextractor is part of a pipeline while if something is wrong, in mode FULL can be helpful. HEADER-SUFFIX is the filename extension for additional headers. In case it is necessary to change o modify the header of the image, it can be created an external header with the same name of the image. Then Sextractor will read the file.head and copy in the original image header. Be careful, if there are double keywords Sextractor writes the external paramters over the old ones.

```
# Default configuration file for SExtractor 2.12.4
# EB 2010-10-10
#
```

```
#----- Catalog -----
-----
```

```
CATALOG_NAME      022416_out.cat # name of the output catalog
CATALOG_TYPE      FITS_LDAC      # NONE,ASCII,ASCII_HEAD, ASCII_SKYCAT,
                               # ASCII_VOTABLE, FITS_1.0 or FITS_LDAC
PARAMETERS_NAME   default.param # name of the file containing catalog
contents
```

```
#----- Extraction -----
```

```
DETECT_TYPE       CCD            # CCD (linear) or PHOTO (with gamma
correction)
DETECT_MINAREA    5              # min. # of pixels above threshold
DETECT_MAXAREA    20            # max. # of pixels above threshold

THRESH_TYPE       RELATIVE       #relative to background RMS
DETECT_THRESH     15             # <sigmas> or <threshold>,<ZP> in
mag.arcsec-2
ANALYSIS_THRESH   15             # <sigmas> or <threshold>,<ZP> in
mag.arcsec-2

FILTER            Y              # apply filter for detection (Y or N)?
FILTER_NAME       default.conv   # name of the file containing the filter

DEBLEND_NTHRESH   32            # Number of deblending sub-thresholds
DEBLEND_MINCONT   0.005         # Minimum contrast parameter for
deblending

CLEAN             Y              # Clean spurious detections? (Y or N)?
CLEAN_PARAM       0.1           # Cleaning efficiency
```

```
#----- WEIGHTing -----
```

```
WEIGHT_TYPE       MAP_WEIGHT     # type of WEIGHTing: NONE, BACKGROUND,
                               # MAP_RMS, MAP_VAR or MAP_WEIGHT
WEIGHT_IMAGE      lignan_mask2.fit # weight-map filename
```

```
#----- FLAGging -----
```

```
FLAG_IMAGE        flag.fits      # filename for an input FLAG-image
FLAG_TYPE         OR              # flag pixel combination: OR, AND, MIN,
MAX
                               # or MOST
```

```
#----- Photometry -----
```

```
PHOT_APERTURES    5              # MAG_APER aperture diameter(s) in pixels
PHOT_AUTOPARAMS   2.5, 2.5       # MAG_AUTO parameters:
<Kron_fact>,<min_radius>
PHOT_AUTOAPERS    0.0,0.0       # <estimation>,<measurement> minimum
apertures
PHOT_FLUXFRAC     0.5
```

```
SATUR_LEVEL       60000.0       # level (in ADUs) at which arises
saturation
```

```

SATUR_KEY          PIPPO          # keyword for saturation level (in ADUs)

MAG_ZEROPOINT     0.0            # magnitude zero-point
MAG_GAMMA         4.0            # gamma of emulsion (for photographic
scans)
GAIN              0.0            # detector gain in e-/ADU
GAIN_KEY          GAIN           # keyword for detector gain in e-/ADU
PIXEL_SCALE       600.0         # size of pixel in arcsec (0=use FITS WCS
info)

#----- Star/Galaxy Separation -----

SEEING_FWHM       1.2            # stellar FWHM in arcsec
STARNNW_NAME      default.nnw    # Neural-Network_Weight table filename

#----- Background -----

BACK_TYPE         AUTO          # AUTO or MANUAL
BACK_VALUE        0.0            # Default background value in MANUAL mode
BACK_SIZE         64             # Background mesh: <size> or
<width>,<height>
BACK_FILTERSIZE   3              # Background filter: <size> or
<width>,<height>

#----- Check Image -----

CHECKIMAGE_TYPE   OBJECTS,APERTURES # can be NONE, BACKGROUND,
BACKGROUND_RMS,
                                     # MINIBACKGROUND, MINIBACK_RMS, -
BACKGROUND,
                                     # FILTERED, OBJECTS, -OBJECTS,
SEGMENTATION,
                                     # or APERTURES
CHECKIMAGE_NAME   obj_022416_out.fits,aper_022416_out.fits # Filename
for the check-image

#----- Memory (change with caution!) -----

MEMORY_OBJSTACK   3000           # number of objects in stack
MEMORY_PIXSTACK   300000        # number of pixels in stack
MEMORY_BUFSIZE    1024          # number of lines in buffer

#----- ASSOCIation -----

ASSOC_NAME        sky.list       # name of the ASCII file to ASSOCIate
ASSOC_DATA        2,3,4          # columns of the data to replicate
(0=all)
ASSOC_PARAMS      2,3,4          # columns of xpos,ypos[,mag]
ASSOC_RADIUS      2.0            # cross-matching radius (pixels)
ASSOC_TYPE        NEAREST        # ASSOCIation method: FIRST, NEAREST,
MEAN,
                                     # MAG_MEAN, SUM, MAG_SUM, MIN or MAX
ASSOCSELEC_TYPE   MATCHED        # ASSOC selection type: ALL, MATCHED or -
MATCHED

#----- Miscellaneous -----

VERBOSE_TYPE      NORMAL         # can be QUIET, NORMAL or FULL
HEADER_SUFFIX     .head          # Filename extension for additional
headers

```

```
WRITE_XML      N          # Write XML file (Y/N)?
XML_NAME      sex.xml    # Filename for XML output
XSL_URL       file:///usr/local/share/sextractor/sextractor.xsl
              # Filename for XSL style-sheet
```

Output Parameters

The parameters of output should be listed in the file called `default.param`. An example of a parameter file is showed in figure 4.8. Parameters in the output catalog can be divided into geometric parameters, photometric parameters, astrometric parameters and fitted parameters. Geometric parameters will tell what shape the object is in (basically how the light of the object is distributed over the pixels of that object) and the photometric parameters tell simply how much light there is. Astrometric parameters give the position of the object in the image, be it in pixels or other coordinates. Fitted parameters are calculated from fitting for instance a PSF to the data of the object. There are a few that do not fall in any of these convenient categories; the catalog number (NUMBER), the flag parameters (FLAGS, IMAFLAGS-ISO, NIMAFLAGS-ISO) and the parameters associated with crosscorrellating catalogs.

About photometric parameters, as said, there are five different ways of determining flux or magnitude; isophotal, isophotal-corrected, automatic, best estimate and aperture. For these work it has been chosen to use aperture and auto. In fact, as figure 4.8 shows, it have been use the parameters FLUX-APER, FLUX-AUTO, MAG-AUTO with each its relative error FLUXERR-APER, FLUXERR-AUTO and MAGERR-AUTO. This choise was dictated by what input parameter Scamp wants in order to arrive at an astrometric solution. The following output parameters, always shown in figure 4.8, concern the astrometry and so the position of the object. XWIN-IMAGE and YWIN-IMAGE, required by Scamp, estimate the position along x and y in pixel. This is an iterative process. The computation starts by initializing the windowed centroid coordinates x_{WIN}^0 and y_{WIN}^0 to their basic x and y isophotal equivalents. Then at each iteration t, x_{WIN} and y_{WIN} are refined using:

$$XWIN^{t+1} = x_{WIN}^{t+1} = x_{WIN}^t + 2 \frac{\sum_{r_i^t < r_{max}} \omega_i^t I_i(x_i - x_{WIN}^t)}{\sum_{r_i^t < r_{max}} \omega_i^t} \quad (4.6)$$

$$YWIN^{t+1} = y_{WIN}^{t+1} = y_{WIN}^t + 2 \frac{\sum_{r_i^t < r_{max}} \omega_i^t I_i(y_i - y_{WIN}^t)}{\sum_{r_i^t < r_{max}} \omega_i^t} \quad (4.7)$$

where

$$\omega_i^t = \exp\left(-\frac{r_i^{(t)2}}{2s_{WIN}^2}\right) \quad (4.8)$$

with

$$r_i^t = \sqrt{(x_i - x_{WIN}^t)^2 + (y_i - y_{WIN}^t)^2} \quad (4.9)$$

and $s_{WIN} = d_{50}/\sqrt{8\ln 2}$. The process stops when the cange in position between two iterations is less than $2 \cdot 10^{-4}$ pixel, a condition which is generally achieved

in about 3 to 5 iterations. These process even if it can be slow, is recommended instead of the isophotal equivalents since the provided measurements are more precise. In fact the precision in centroiding offered by windows parameters is very close to that of PSF-fitting.

ALPHAWIN-J2000 and DELTAWIN-J2000 are the RA and DEC coordinates in the windowed, in degrees. After the first order moments are calculated, X2WIN-IMAGE, Y2WIN-IMAGE and XYWIN-IMAGE can be obtained as second order moments. Here they are the equations:

$$X2WIN = \overline{x_{WIN}^2} = \frac{\sum_{r_i < r_{max}} w_i I_i (x_i - \overline{x_{WIN}})^2}{\sum_{r_i < r_{max}} w_i I_i} \quad (4.10)$$

$$Y2WIN = \overline{y_{WIN}^2} = \frac{\sum_{r_i < r_{max}} w_i I_i (y_i - \overline{y_{WIN}})^2}{\sum_{r_i < r_{max}} w_i I_i} \quad (4.11)$$

$$XY2WIN = \overline{xy_{WIN}} = \frac{\sum_{r_i < r_{max}} w_i I_i (x_i - \overline{x_{WIN}})(y_i - \overline{y_{WIN}})}{\sum_{r_i < r_{max}} w_i I_i} \quad (4.12)$$

$$ERRX2WIN = var(\overline{x_{WIN}}) = 4 \frac{\sum_{r_i < r_{max}} w_i^2 \sigma_i^2 (x_i - \bar{x})^2}{(\sum_{r_i < r_{max}} w_i I_i)^2} \quad (4.13)$$

$$ERRY2WIN = var(\overline{y_{WIN}}) = 4 \frac{\sum_{r_i < r_{max}} w_i^2 \sigma_i^2 (y_i - \bar{y})^2}{(\sum_{r_i < r_{max}} w_i I_i)^2} \quad (4.14)$$

$$ERRXYWIN = cov(\overline{y_{WIN}}, \overline{x_{WIN}}) = 4 \frac{\sum_{r_i < r_{max}} w_i^2 \sigma_i^2 (x_i - \overline{x_{WIN}})(y_i - \overline{y_{WIN}})}{(\sum_{r_i < r_{max}} w_i I_i)^2} \quad (4.15)$$

AWIN-IMAGE, BWIN-IMAGE and THETAWIN-J2000 are respectively the minor axis, the major axis and the position angle of an ellipse, derived from the moments. These parameters are intended to describe the detected object as an elliptical shape. Follows the equation from the manual [3]:

$$A^2 = \frac{\overline{x^2} + \overline{y^2}}{2} + \sqrt{\left(\frac{\overline{x^2} - \overline{y^2}}{2}\right)^2 + \overline{xy}^2} \quad (4.16)$$

$$B^2 = \frac{\overline{x^2} + \overline{y^2}}{2} - \sqrt{\left(\frac{\overline{x^2} - \overline{y^2}}{2}\right)^2 + \overline{xy}^2} \quad (4.17)$$

$$ERRA^2 = \frac{var(\bar{x}) + var(\bar{y})}{2} + \sqrt{\left(\frac{var(\bar{x}) - var(\bar{y})}{2}\right)^2 + cov^2(\bar{x}, \bar{y})} \quad (4.18)$$

$$ERRB^2 = \frac{var(\bar{x}) + var(\bar{y})}{2} - \sqrt{\left(\frac{var(\bar{x}) - var(\bar{y})}{2}\right)^2 + cov^2(\bar{x}, \bar{y})} \quad (4.19)$$

$$\tan(2 \times ERRTHETA) = 2 \frac{cov(\bar{x}, \bar{y})}{var(\bar{x}) - var(\bar{y})} \quad (4.20)$$

From these shape parameters, ELONGATION can be derived as

$$ELONGATION = \frac{A}{B} \quad (4.21)$$

Lastly there are the parameters VIGNET and FLUX-RADIUS. With the first it can be obtained the pixel data around detection and this gives an idea of the PSF width in the case of stars. While the last parameters is the efferctive radius, this is the term commonly used to define the point in a light profile within which encloses half the flux from an object. In the case of SExtractor, several radii can be defined (input parameter PHOT-FLUXFRAC).

```

NUMBER                #Running object number
FLUX_APER              #Flux vector within fixed circular aperture(s)
[count]
FLUXERR_APER          #RMS error vector for aperture flux(es) [count]
FLUX_AUTO             #Flux within a Kron-like elliptical aperture
[count]
FLUXERR_AUTO         #RMS error for AUTO flux [count]
MAG_AUTO              #Kron-like elliptical aperture magnitude [mag]
MAGERR_AUTO          #RMS error for AUTO magnitude [mag]
XWIN_IMAGE            #Windowed position estimate along x [pixel]
YWIN_IMAGE            #Windowed position estimate along y [pixel]
ALPHAWIN_J2000       #Windowed right ascension (J2000) [deg]
DELTAWIN_J2000       #Windowed declination (J2000) [deg]
X2WIN_IMAGE           #Windowed variance along x [pixel**2]
Y2WIN_IMAGE           #Windowed variance along y [pixel**2]
XYWIN_IMAGE          #Windowed covariance between x and y [pixel**2]
AWIN_IMAGE            #Windowed profile RMS along major axis [pixel]
BWIN_IMAGE            #Windowed profile RMS along minor axis [pixel]
THETAWIN_J2000       #Windowed position angle(east of north) (J2000)
[deg]
ERRRAWIN_IMAGE       #RMS windowed pos error along major axis [pixel]
ERRBWIN_IMAGE        #RMS windowed pos error along minor axis [pixel]
ERRTHETAWIN_IMAGE    #Windowed error ellipse pos angle (CCW/x) [deg]
SNR_WIN              #Extraction flags
FLAGS                #Weighted extraction flags
FLAGS_WEIGHT         #A IMAGE/B IMAGE
ELONGATION            #Pixel data around detection [count]
VIGNET(10,10)        #Fraction-of-light radii [pixel]
FLUX_RADIUS
    
```

Figure 4.8: This is an example of a file of parameter, default.param, used in this work. It is a list of parameters chosen to be calculated and written in the output catalog.

4.2.2 Scamps

SExtractor has created a catalog of point sources for each image, now these catalogs will be read by Scamp. Then Scamp approximate astrometric data, compute a proper astrometric and photometric solution and finally save the result of this calibration in header files. The work can be summarized into the following steps (figure 4.9 shows the procedure):

1. Input: catalogs and headers are read and checked for content. Scamp sorts catalogs by position on the sky ("group of fields") as well as astrometric and photometric contexts ("instrument").
2. Mosaics of detectors undergo a specific pre-treatment to homogenise the astrometric calibration across the focal plane.
3. A catalog of astrometric standards ("reference catalog") is downloaded from the Vizier database [5] for every group.
4. The reference catalog are utilised by a pattern matching procedure to register al input catalog.
5. All detections and reference sources are cross-matched and an strometric solution is computed. This operation is repeated after clipping of outliers.
6. A photometric solution is computed in two passes (and outliers are clipped at each iteration).
7. Updated astrometric and photometric calibration data are written to external headers.

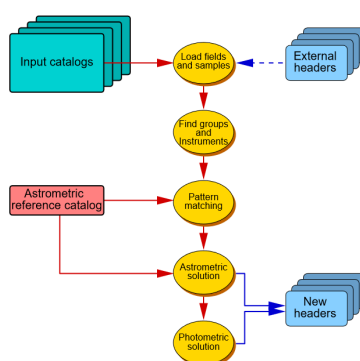


Figure 4.9: The figure shows which steps scamp undergoes to arrive at an astrometric and photometric solution.

To work Scamp has to have a good file of configuration, `scamp.conf`. The configuration file used for these work is illustrated in the following pages.

```

# Default configuration file for SCAMP 2.6.2
# EB 2017-11-06
#

#----- Reference catalogs -----

REF_SERVER          vizier.u-strasbg.fr # Internet addresses of catalog
servers

                                # Possible mirrors include:
                                # vizier.nao.ac.jp,
                                # vizier.hia.nrc.ca,
                                # vizier.ast.cam.ac.uk,
                                # vizier.iucaa.ernet.in,
                                # vizier.china-vo.org,
                                # vizier.cfa.harvard.edu and
                                # viziersaao.chpc.ac.za
REF_TIMEOUT         10                # Server connection timeouts (s)
0=none
ASTREF_CATALOG      TYCHO-2           # NONE, FILE, USNO-A2, USNO-B1, GSC-
2.3,

                                # TYCHO-2, UCAC-4, URAT-1, NOMAD-
                                # CMC-15, 2MASS, DENIS-3, SDSS-
                                # GAIA-DR1 or ALLWISE
                                # Photom. band for
ASTREF_BAND         DEFAULT           # or DEFAULT, BLUEST, or REDDEST
astr.ref.magnitudes

ASTREFCAT_NAME      astrefcat.cat     # Local astrometric reference
catalogs
ASTREFCENT_KEYS     X_WORLD, Y_WORLD # Local ref.cat. centroid
parameters
ASTREFERR_KEYS      ERRA_WORLD, ERRB_WORLD, ERRTHETA_WORLD
                                # Local ref.cat. err. ellipse
params
ASTREFMAG_KEY       MAG               # Local ref.cat. magnitude
parameter
ASTREFMAGERR_KEY    MAGERR            # Local ref.cat. mag. error
parameter
ASTREFOBSDATE_KEY   OBSDATE           # Local ref.cat. obs. date
parameter
ASTREFMAG_LIMITS   0.0, 4.0         # Select magnitude range in
ASTREF_BAND         SAVE_REFCATALOG   # Save ref catalogs in FITS-LDAC
format?
REFOUT_CATPATH      .                 # Save path for reference catalogs

#----- Merged output catalogs -----

MERGEDOUTCAT_TYPE   NONE              # NONE, ASCII_HEAD, ASCII,
FITS_LDAC
MERGEDOUTCAT_NAME    merged.cat        # Merged output catalog filename

#----- Differential geometry maps -----

SAVE_DGEOMAP        N                # Save differential geometry maps
(Y/N)?
DGEOMAP_NAME        dgeo.fits         # Differential geometry map
filename
DGEOMAP_STEP        2                # Map sampling step

```


ASTRACCURACY_KEY param.	ASTRACCU	# FITS keyword for ASTR_ACCURACY
ASTR_ACCURACY parameter	0.1	# Astrom. uncertainty floor
ASTRCLIP_NSIGMA sigmas	3.0	# Astrom. clipping threshold in
COMPUTE_PARALLAXES (Y/N)?	N	# Compute trigonom. parallaxes
COMPUTE_PROPERMOTIONS	N	# Compute proper motions (Y/N)?
CORRECT_COLOURSHIFTS	N	# Correct for colour shifts (Y/N)?
INCLUDE_ASTREFCATALOG (Y/N)?	Y	# Include ref.cat in prop.motions
ASTR_FLAGSMASK FLAGS	0x00fc	# Astrometry rejection mask on SEx
ASTR_IMAFLAGS IMAFMASK	0x0	# Astrometry rejection mask on
#----- Photometric solution -----		
SOLVE_PHOTOM (Y/N)?	Y	# Compute photometric solution
MAGZERO_OUT output	0.0	# Magnitude zero-point(s) in
MAGZERO_INTERR	0.01	# Internal mag.zero-point accuracy
MAGZERO_REFERR accuracy	0.03	# Photom.field mag.zero-point
PHOTINSTRU_KEY photom.	FILTER	# FITS keyword(s) defining the
MAGZERO_KEY point	PHOT_C	# FITS keyword for the mag zero-
EXPOTIME_KEY time (s)	ONTIME	# FITS keyword for the exposure
AIRMASS_KEY	AIRMASS	# FITS keyword for the airmass
EXTINCT_KEY coeff	PHOT_K	# FITS keyword for the extinction
PHOTOMFLAG_KEY flag	PHOTFLAG	# FITS keyword for the photometry
PHOTFLUX_KEY measurement	FLUX_AUTO	# Catalog param. for the flux
PHOTFLUXERR_KEY error	FLUXERR_AUTO	# Catalog parameter for the flux
PHOTCLIP_NSIGMA sigmas	3.0	# Photom.clipping threshold in
PHOT_ACCURACY (frac.)	1e-3	# Photometric uncertainty floor
PHOT_FLAGSMASK FLAGS	0x00fc	# Photometry rejection mask on SEx
PHOT_IMAFLAGS IMAFMASK	0x0	# Photometry rejection mask on
#----- Source selection -----		
SN_THRESHOLDS and	1.0,10.0	# S/N thresholds (in sigmas) for all # high-SN sample
FWHM_THRESHOLDS sources	0.5,10.0	# FWHM thresholds (in pixels) for
ELLIPTICITY_MAX	0.5	# Max. source ellipticity
FLAGS_MASK FLAGS	0x00f0	# Global rejection mask on SEx

```

WEIGHTFLAGS_MASK      0x00ff      # Global rejec. mask on SEx
FLAGS_WEIGHT
IMAFLAGS_MASK         0x0         # Global rejec. mask on SEx
IMAFLAGS_ISO

#----- WCS headers -----

AHEADER_GLOBAL        scamp.ahead   # Filename of a global input
header
AHEADER_NAME          # List of input header filenames
# (overrides AHEADER_SUFFIX)
AHEADER_SUFFIX        .ahead       # Filename extension for
additional
# input headers
HEADER_NAME           # List of output header filenames
# (overrides HEADER_SUFFIX)
HEADER_SUFFIX         .head        # Filename extension for output
headers
HEADER_TYPE           NORMAL       # NORMAL or FOCAL_PLANE

#----- Check-plots -----

CHECKPLOT_CKEY        SCAMPCOL     # FITS keyword for PLPLOT field
colour
CHECKPLOT_DEV         PNG          # NULL, XWIN, TK, PS, PSC, XFIG,
PNG,
# JPEG, AQT, PDF or SVG
CHECKPLOT_RES         0           # Check-plot resolution (0 =
default)
CHECKPLOT_ANTIALIAS   Y           # Anti-aliasing using convert
(Y/N) ?
CHECKPLOT_TYPE        FGROUPS,DISTORTION,ASTR_INTERROR2D,ASTR_INTERROR1D,ASTR_REFERROR2D,ASTR_R
EFERROR1D,ASTR_CHI2,PHOT_ERROR,ASTR_XPIXERROR2D,ASTR_YPIXERROR2D,ASTR_SB
PIXERROR1D
CHECKPLOT_NAME        fgroups,distort,astr_interror2d,astr_interror1d,astr_referror2d,astr_refe
rror1d,astr_chi2,psphot_error,astr_xpixmap2d,astr_ypixmap2d,astr_subp
ixerror1d # Check-plot filename(s)

#----- Check-images -----

CHECKIMAGE_TYPE       #AS_XCORR,AS_PAIR,AS_REFPAIR,LL_XCORR,LL_PAIR,
LL_REFPAIR,
# NONE, AS_PAIR, AS_REFPAIR, or AS_XCORR
CHECKIMAGE_NAME       check-as-xcorr.fits,check-as-pair.fits,check-as-
refpair.fits,check-ll-xcorr.fits,check-ll-pair.fits,check-ll-refpair.fits
# Check-image filename(s)

#----- Miscellaneous -----

VERBOSE_TYPE          NORMAL       # QUIET, NORMAL, LOG or FULL
WRITE_XML             Y           # Write XML file (Y/N)?
XML_NAME              scamp.xml    # Filename for XML output
XSL_URL              file:///usr/local/share/scamp/scamp.xsl
# Filename for XSL style-sheet
NTHREADS              0           # Number of simultaneous threads
for
# the SMP version of SCAMP
# 0 = automatic

```

In detail, how scamp works. The first keywords that can be seen in the previous pages regard all setting of the catalog of reference. There are different reference catalog that can be downloaded. It all depends what field is taken in study. In this case, the catalog TYCHO-2 has been chosen because the images that had to be calibrated are stars in a large field of view (> 10 deg). Since the reference catalog has billion of stars it can be chosen to clip the catalog in magnitude. This can be done with the keyword `ASTREFMAG-LIMIT`, since the stars in the images taken are between magnitudes -4 and 4, it was taken a magnitude range of 0.0 and 4.0. After Scamp set the names for an eventual merge catalog if there is one, it can be saved a differential geometry maps if wanted and set the name for a full output catalog where the parameter in the reference catalog and the new are all written. The second step is the pattern matching. Before starting the match, when the keyword `MATCH` is set to `Y`, Scamp undergoes under a pre-processing of mosaics. The keyword `MOSAIC-TYPE` set the type of pre-processing. In the first run Scamp is set to `LOOSE` because the mosaic is totally uncalibrated. This mode makes all detector positions to be considered as independent between exposure. Then the mathing begins, firstly correction to pixel scale and position angle are computed. Basically Scamp uses the technique described by Kaiser et al. (1999): histograms of source pairs in $\log(\text{distance})$ vs position-angle space are calculated for the reference catalog and for the catalog to be matched. Both histograms are then cross-correlated and bandpass-filtered using Fast Fourier Transforms. A peak finder algorithm locates the correlation peak, whose coordinates correspond to the relative position-angle and $\log(\text{scalefactor})$ between the two catalogs. A "contrast" factor is computed in order to asses the reliability of the correlation: it is defined as the ratio of the amplitude of the detected peak (within the allowed limits in pixel scale and position angle) to the amplitude of the second highest peak found in the cross-correlation. Usually a contrast factor > 1 is taken as a good value. The recovery of true pixel scale and position angle corrections is controlled with the keywords `MATCH-NMAX`, `MATCH-RESOL`, `PIXESCALE-MAXERR` and `POSANGLE-MAXERR`. The first keyword set the maximum number of unsaturated sources that should be used for searching the pixel scale and position angle. It has be set to default 0, so that matching is first attempted with 2000 sources, and then increased by a factor of 2 until the contrast increases. The algorithm currently stops at 8000. The second keyword sets the resolution of the 2D histograms (in arcsec per pixel). This parameter has been set to 1000 arcsec per pixel because the input catalogs has a large field of view with a low number of stars detected. `PIXELSCALE-ERROR` is the keyword that sets the search range for the scaling factor. The default is 1.2, which means a search range of $\pm 20\%$ with respect to the pixel scale quoted in the original header. In practice, search ranges up to 2 can be requested, like in this case it has been chosen to set a value of 1.7.

POSANGEL-MAXERR sets the search range for the image orientation. It has been set to 30 which means a search range of $\pm 30^\circ$.

Once the pixel scale and position angle have been corrected, the shift in right ascension and declination between the catalog to be matched and the reference catalog is computed by cross-correlating the 2D histograms of projected source positions in both catalogs.

Like it has been said until now, Scamp makes heavy use of cross-identification between the various catalogs at several stages. The radius of the cross-identification is set by the keyword CROSSID-RADIUS, in arcsec. Since the field of view of the camera in study is about 180 degrees, after different try the parameter has been set to 3000 arcsec.

The principle underlying the astrometric solution

The astrometric solution is the result of a χ^2 minimisation. The adopted χ^2 is the quadratic sum of differences in position between overlapping detections from pairs of fields. One of those fields may be a reference field, or both may be uncalibrated. In both cases, coordinates used in the differences are reprojected coordinates ξ , common to all fields of a same group. The ξ 's are derived from the measured detector coordinates x , and reprojection operator $\chi(x)$ is different for each field, and even each set. Minimising (4.22) leads to a solution which adjusts best (in the χ^2 sense) all the various fields together while tightening the whole group to the reference catalogue:

$$\chi^2 = \sum_s \sum_a \sum_{b>a} \omega_{s,a,b} \| \xi_a(x_{s,a}) - \xi_b(x_{s,b}) \|^2 \quad (4.22)$$

where $\omega_{s,a,b}$ is the non zero weight for the pair of detections in fields a and b related to source s:

$$\omega_{s,a,b} = \frac{1}{\sigma_{s,a}^2 + \sigma_{s,b}^2} \quad (4.23)$$

$\sigma_{s,f}$ is the positional uncertainty for source s in field f.

For mosaic cameras, a catalog comprises several sub-catalog for each field: one per detector chip. The reprojection operator, $\xi_{c,f}$, for chip c and field f, is expressed as a combination of an undistorted reprojection operator $\xi_{c,f}^0$ derived from the (tangential) projection approximated at the initial matching stage, and two decompositions over linear suspases describing instrumental distortions as deformations of the pixel grid:

$$\xi_{c,f}(x) = \xi_{c,f}^0(x + \sum_p c_{i,p} \phi_p(o) + \sum_m d_{f,m} \psi_m(\rho)) \quad (4.24)$$

The vector χ represents the context of observation of a given source. The components of χ may affect the projection distortion at the current position on the field. In general, χ will include at least the current coordinate vector x since distortion on a focal plane is position-dependent. It may also contain field-dependent parameters like airmass or time. The components of the vector χ are selected using the DISTOR-KEYS configuration parameter. The arguments can be names of SExtractor measurements, or keywords from the image fits headers representing numerical values. The DISTOR-KEYS used have been XWIN-IMAGE and YWIN-IMAGE (from SExtractor).

The basis functions ϕ_p are simple polynomials of the components of χ . Each of these components χ_l belongs to a distortion group $g = 0, 1, \dots, N_G$, such that

$$\phi_p(\chi) = \prod_{g < N_g} \left(\prod_{(\sum_{l \in \Lambda_g} d_l) \leq D_g} \chi_l^{d_l} \right) \quad (4.25)$$

where Λ_g is the set of contexts l that belongs to the distortion group g , and D_g is the polynomial degree of group g . Index p runs over all possible combinations of the d_l and g . The DISTORT-GROUPS configuration parameters in combination with the DISTOR-KEYS must be filled in to indicate which distortion group each component of χ belongs to. The default for DISTORT-GROUPS is 1,1 meaning that both DISTOR-KEYS belong to the same unique distortion group. The polynomial degrees D_g are set with DISTOR-DEGREES. After several trials it has been chosen to set this keyword to 3, meaning a 3rd degree polynomial.

The following figure 4.10 is the check plot DISTORTION showing the pixel scale over the field of view, in this case it can be seen that the scale decreases from left to right.

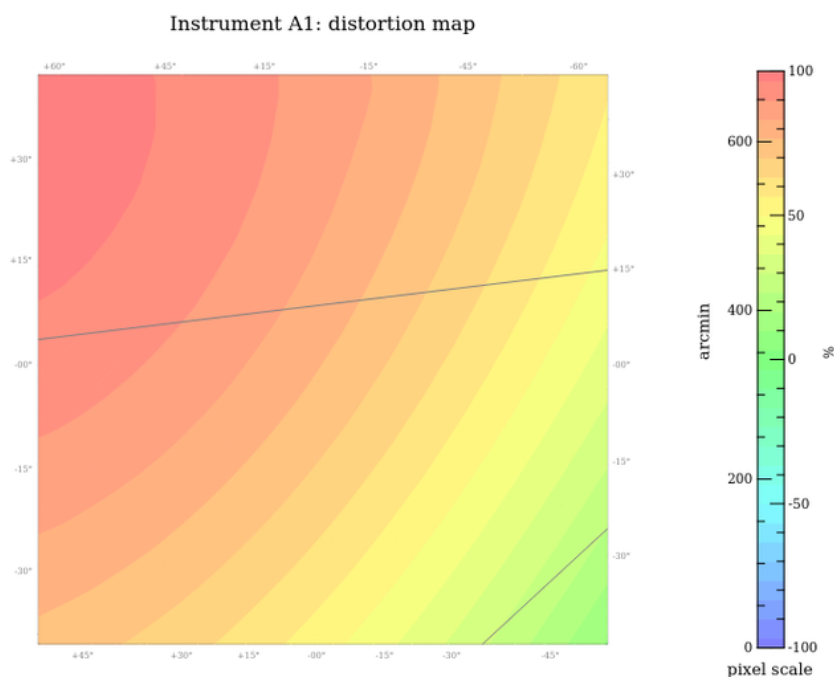


Figure 4.10: This is a chart showing for each astrometric instrument an astrometric model of the input frame(s) after calibration. The pixel size is represented over the field of view using a colour scale ranging from blue to red.

The last procedure to take in account while finding an astrometric solution is the possible blending of mismatched detections. It is important to eliminate as many false detections as possible from the input catalog. So in Scamp can be performed a clipping at ASTRCLIP-NSIGMA standard deviations after computing a first astrometric solution. Since the input catalog has been extracted well it has been chosen to set the clipping at its default value, 3, i.e., Scamp eliminates 1 to 3% of sources in typical conditions. After clipping, a new cross-identification is done, and the final astrometric solution is finally computed.

Photometric solution

After finding an astrometric solution, Scamp follows with finding the photometric solution. In input the software wants one flux measurement and is associated uncertainty for every detection. The names of the columns containing both quantities in the input catalogues can be specified with the PHOTFLUX-KEY and PHOTFLUXERR-KEY configuration parameters. The default measurements are SExtractor's FLUX-AUTO and FLUXERR-AUTO . The flux measurements f are

assumed to be in ADUs, that is, in units of pixel values. To allow photometric measurements to be compared between exposures under various observing conditions or even between different instruments, the instrumental fluxes read in the input catalogs are converted to magnitudes with

$$m = -2.5 \log_{10} f + m_0 + 2.5 \log t + c_a a \quad (4.26)$$

where m_0 is the instrumental zero point for a 1 second exposure, t is the exposure time, c_a is the extinction coefficient at unit airmass and a is the average exposure airmass.

In principle, the photometric solution is the result of a χ^2 minimisation. The adopted χ^2 is the quadratic sum of differences in magnitude between overlapping detections from pairs of exposures observed with the same photometric instrument. Minimising (4.27) leads to a solution which adjusts best (in the χ^2 sense) all the various fields together while tightening the whole group to the photometric field zero point:

$$\chi^2 = \sum_s \sum_a \sum_{b>a} w_{s,a,b} (Z_a + m_{s,a} - Z_b - m_{s,b})^2 \quad (4.27)$$

where $w_{s,a,b}$ is given in equation 4.23 (it is the non-zero weight for the pair of detections in fields a and b related to source s) where ω_{sab} is the non zero weight for the pair of detections in fields a and b related to source s .

First and Second run of Scamp

Scamp to arrive at an acceptable astrometric solution has to be run twice. In the first run all parameters are set as described in the previous paragraphs, except for the keyword MOSAIC-TYPE. In the first run it is set to LOOSE, in this way the software is set free to change and find the best parameter for CRPIX1 and CRPIX2, i.e. the center of the image.

These parameters has been given in input with an external .aheder file, called scamp.aheder, see figure 4.11. In this file, besides the CRPIX parameters, also the CDs parameters are set. These values are related to the scale of the CCD. To obtain a scale about $600''$ the initial input value is 0.19 in degrees per pixel. Other values has been tested to arrive at a better solution but in the end the value chosen, 0.19, has been found as the best.

```

EQUINOX =          2000.0      / Mean equinox
CTYPE1  = 'RA---ARC'         / Projection and reference system
CTYPE2  = 'DEC--ARC'         / Projection and reference system
CRPIX1  = 640
CRPIX2  = 480
CD1_1   =                  0.19 / deg/pix
CD1_2   =                  0.0 / deg/pix
CD2_1   =                  0.0 / deg/pix
CD2_2   =                 -0.19 / deg/pix
END

```

Figure 4.11: The figure shows the file .aheder used for the first run of Scamp. The CRPIXs are the parameters indicating the center of the image in pixels, while CDs are the parameters related to the scale.

When the run is completed with this mode, it will be taken the calculated CRPIX1 and CRPIX2 (coordinates in pixel of the center) from the output header of the input catalog with the best contrast, see figure 4.12.

Group 1: 161 standards in TYCHO-2 (band VT)								
	instruments	pos.angle	scale	cont.	shift	cont.		
000123_out.cat	A1	P1	+0.00 deg	608.7"	0.856	+1.9e+04"	-2.0e+04"	0.843
235637_out.cat	A1	P1	+0.00 deg	608.7"	0.892	+2.0e+04"	-1.9e+04"	0.516
234625_out.cat	A1	P1	+3.38 deg	567.8"	1.01	+6.8e+03"	-2.6e+04"	0.189
234632_out.cat	A1	P1	+7.63 deg	559.5"	1.03	+2.6e+04"	+7.8e+03"	0.473
000657_out.cat	A1	P1	+0.00 deg	608.7"	0.902	+2.2e+04"	-1.6e+04"	0.594
001136_out.cat	A1	P1	+4.04 deg	628.2"	1.03	+3.6e+04"	-2.1e+04"	1.03
233612_out.cat	A1	P1	+0.00 deg	608.7"	0.996	+1.4e+04"	-3.0e+04"	0.567
233620_out.cat	A1	P1	+3.50 deg	567.7"	1.03	-2.8e+04"	+5.0e+03"	0.172
001709_out.cat	A1	P1	+14.57 deg	618.1"	1.02	-2.9e+04"	-1.0e+04"	0.623
232600_out.cat	A1	P1	+0.00 deg	608.7"	0.853	-7.2e+03"	+1.3e+04"	0.519
232607_out.cat	A1	P1	+0.00 deg	608.7"	0.942	-9.5e+03"	+9.5e+03"	0.520
002721_out.cat	A1	P1	+0.00 deg	608.7"	0.994	+2.9e+04"	-5.6e+03"	0.424
231548_out.cat	A1	P1	+0.00 deg	608.7"	0.885	+8.4e+03"	-4.0e+04"	0.525
003734_out.cat	A1	P1	+4.95 deg	570.6"	1.13	+1.3e+04"	-2.1e+04"	0.544
230535_out.cat	A1	P1	-20.28 deg	633.3"	1.22	-6.6e+04"	+2.4e+04"	0.773
004746_out.cat	A1	P1	+0.00 deg	608.7"	0.933	+3.8e+04"	+4.0e+03"	0.880
005758_out.cat	A1	P1	+0.00 deg	608.7"	0.934	+4.2e+04"	+9.0e+03"	0.784

Figure 4.12: The figure shows part of the results when scamp is run the first time.

Then Scamp is run another time with the new scamp.aheder with MOSAIC-TYPE set to UNCHANGED, this means that the software is forced to take in the set parameters without much freedom as in LOOSE mode.

To check how the calibration has worked, another check plot has been created with scamp. In the figure 4.13 , ASTR-CHI2 shows internal and reference χ^2 per degree of freedom of the astrometric solution as a function of catalog sequence number.

CHAPTER 4. ASTROMETRIC CHARACTERIZATION OF PRISMA CAMERAS70

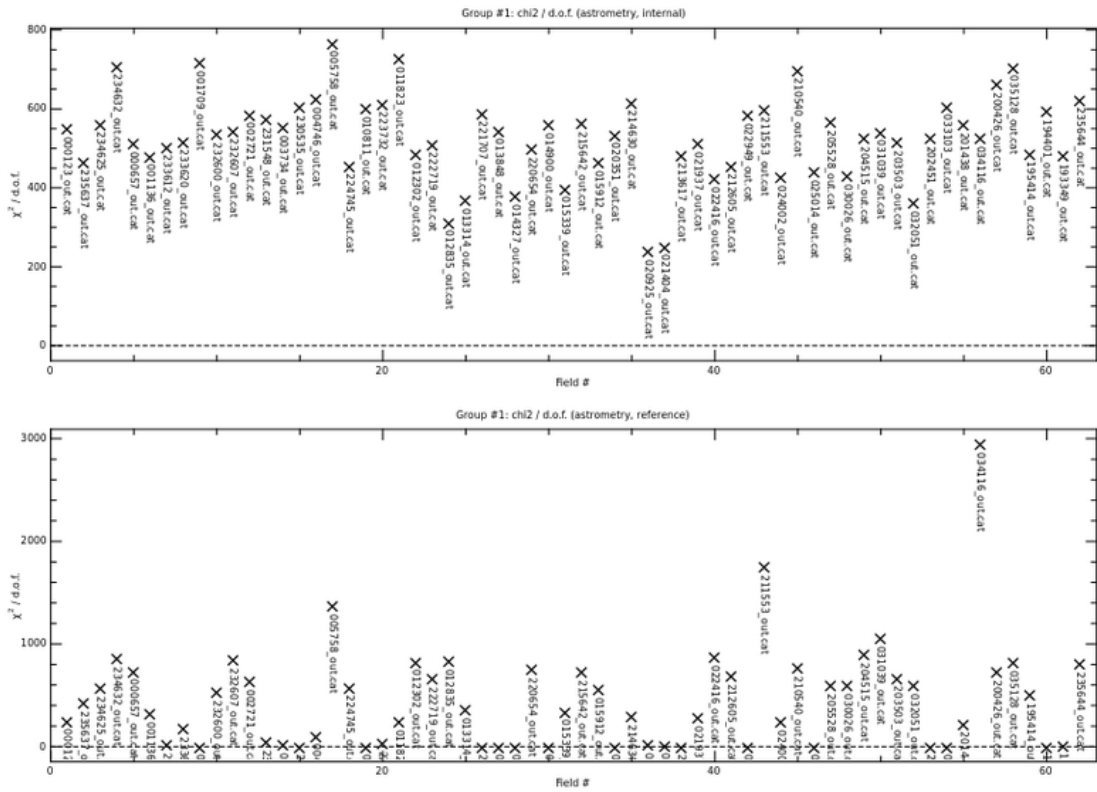


Figure 4.13: In the figure χ^2 of the internal catalog and the reference are compared, it can be seen that in general both values fluctuate about 200 and 800.

4.3 Results

After running Sextractor on the data from two different stations, that had detected an event, they has been obtained 62 catalogs for Lignan station and 68 catalogs for Torino station. Both sets of catalogs has been run with Scamp twice, like it has been explained in the previous sections. At the end of the second run with Scamp 62 headers for Lignan and 68 headers for Torino has been created. At this point to apply the astrometric solution to the image of the meteor, it has been taken the header nearer in time at the event. Before applying at all the event's images the header with Sextractor. To verify the congruency of the solution it has been apply the output header to the relative image. In the following figure 4.14 it is shown the coordinate of α Ursa Maior, from refernce catalog RA is 11h 04min and DEC 61°38' and the result of the astrometry with RA 11h 33min and DEC 61°29'. In the end it has been achieved a discreet agreement.

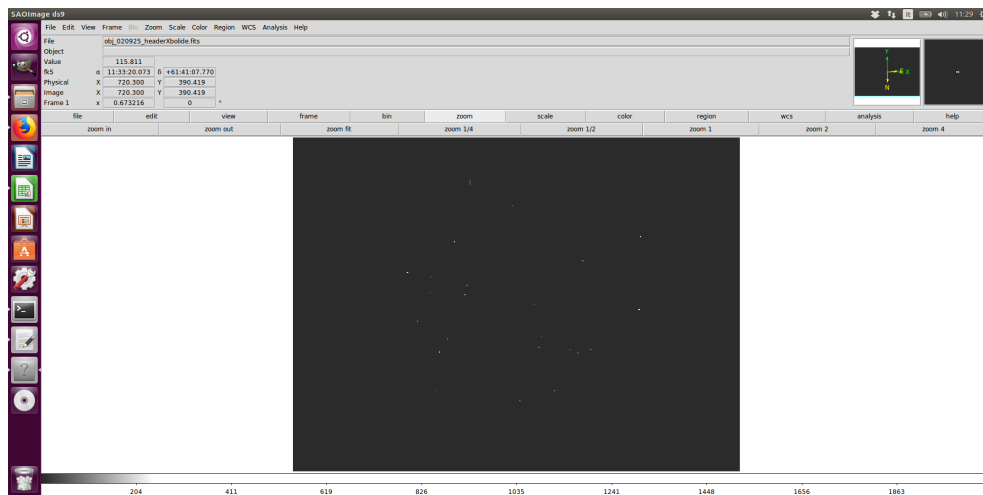


Figure 4.14: In the figure it is shown the application of the astrometric solution to a calibration image to verify that the stars are well recognized. The cursor points alpha Ursa Maior. Moreover it is verified that the orientation of the axis is so that North point south and East towards right.

This error comes from both Scamp and Sextractor. In the case of Scamp the error on the alpha and declination is of the order of about 10^{-2} , a sample of the values are shown in table 4.1 , they are extrapolated from the output full catalog created by Scamp at the end of the process.

ALPHAJ2000	DELTAJ2000	ERRA	ERRB
63.78	-12.49	1.69e-02	1.69e-02
63.59	-12.59	1.70e-02	1.70e-02
15.01	-2.07	1.73e-02	1.73e-02
4.66	-2.60	2.43e-02	2.43e-02
4.46	-2.09	2.49e-02	2.49e-02
16.49	-0.84	1.69e-02	1.69e-02
16.20	-0.52	1.69e-02	1.69e-02
63.90	-1.72	1.70e-02	1.70e-02
15.94	11.58	1.69e-02	1.69e-02
15.58	11.92	1.69e-02	1.69e-02
36.62	16.58	1.69e-02	1.69e-02
44.96	16.13	1.69e-02	1.69e-02
44.96	16.13	1.69e-02	1.69e-02
44.96	16.13	1.69e-02	1.69e-02
12.17	18.02	1.69e-02	1.69e-02

Table 4.1: In this table is shown a part of the output file that Scamp creates after the final run. In the first column is the AlphaJ2000, the second is DeltaJ2000 and the last column are the errors respectively calculated by Scamp(all expressed in decimal degrees).

When it is sure that the stars in the field of view are well recognized, then the solution is applied to the event images. To do this, the output header of Scamp chosen is renamed as each event image. Be careful, before running SExtractor to copy the external header to the image, it is important to eliminate the keywords CRVAL1 and CRVAL2, in this way they are left the right parameters in the original FITS header. So SExtractor is run over all the event image with their external header. In output there will be a catalog for each image with the coordinate and other parameter. An example of the output is in table 4.2.

RA DD	DEC DD	VARIANCE DD	VARIANCE DD
121.4947	-2.2575	3.0734e-04	3.7616e-04
120.9354	-2.1014	1.7385e-04	2.1215e-04
120.4320	-1.9267	1.3319e-04	1.6207e-04
119.8583	-1.7515	1.0122e-04	1.2271e-04
119.2986	-1.5737	2.9842e-05	3.6091e-05
118.7864	-1.4220	1.7758e-05	2.1412e-05
118.2022	-1.2261	1.2393e-05	1.4883e-05
117.6435	-1.0629	1.0087e-05	1.2072e-05
117.0706	-0.8963	1.0677e-05	1.2743e-05
116.5022	-0.7003	1.0906e-05	1.2978e-05
115.9016	-0.5283	1.1328e-05	1.3440e-05
115.3338	-0.3600	2.4198e-05	2.8627e-05
114.7104	-0.1411	3.5163e-05	4.1466e-05
114.1660	+0.0354	1.0484e-04	1.2325e-04
113.5191	+0.2412	1.2275e-04	1.4382e-04

Table 4.2: This table shows in the first column the RA in decimal degrees, in the second DEC in decimal degrees and the last two column are the errors in decimal degrees calculated by SExtractor after apply the headers to the event images

The errors that are produced by each software have to be sum and they give rise at the discrepancy which is translate in an order of 10 minutes in the position, like it was illustrated previously. This error has to take in account in even if it is not particulary great because it will affect the result in the calculation of the meteoric trajectory.

Chapter 5

Calculation of meteoric trajectories

5.1 Theory for the calculation of fireball trajectory

The last step is to compute the projection of any measured point of the fireball trajectory onto the average fireball trajectory as defined from two stations. To do this it is been taken as reference Ceplecha 1987 [6]. After each point of the fireball trail is measured, the average trajectory can be written as

$$a\xi_i + b\eta_i + c\zeta_i = 0 \quad (5.1)$$

Substituting a,b,c into the rectangular geocentric system of coordinates written for station A, yields the geocentric position of the plane containing the station A and the trajectory:

$$a_A\xi + b_A\eta + c_A\zeta + d_A = 0 \quad (5.2)$$

where d is the distance of the plane from the Earth's center. So the pair of stations now define two planes, each plane containing the fireball trajectory. The intersection of these two planes is exactly the fireball trajectory as defined by the fireball photographs taken from these two stations. From 5.2, it can be derived the intersection of these two planes. Other than the coordinates it is needed the value of the angle Q of the two planes given by their normal vectors (a_A, b_A, c_A) , (a_B, b_B, c_B) .

$$\cos Q_{AB} = | a_A a_B + b_A b_B + c_A c_B | : ((a_A^2 + b_A^2 + c_A^2)(a_B^2 + b_B^2 + c_B^2))^{1/2} \quad (5.3)$$

The next task is to find the best perpendicular projection of the points of the trajectory measured on the station A record onto the average fireball trajectory

defined by ξ_R, η_R, ζ_R computed the intersection of the planes. The position of A and a point on the trajectory defines a straight line deviating somewhat from the plane (station A, fireball trajectory). It is defined the plane perpendicular to the plane and containing the straight line. The intersection of this plane with the fireball trajectory is the point that is searched. After several steps that are described in the original paper [6]. At the end of the process it will arrive at the compute of the distances, l_n , along the fireball trajectory from the first mark:

$$l_n = [(X_n - X_1)^2 + (Y_n - Y_1)^2 + (Z_n - Z_1)^2]^{1/2} \quad (5.4)$$

and analyze these distances as function of time and determine velocities and accelerations at any point of the fireball trajectory.

Having l_n, \bar{h}_n for each t_n , different methods can be use to compute the best fit of them as functions of time. The preferable method is the exact solution of the single-body motion equations of meteor physics (Pecina and Ceplecha, 1983, 1984). The initial velocity, v_∞ , and the radiant define the initial velocity vector, which is used for the meteoroid orbit computations together with the average velocity, \bar{v} , at the average point somewhere in the middle of the average trajectory.

5.2 Triangulation results for two stations

So after obtaining the coordinates of the points of the fireball with Sextractor and Scamp, it can be computed the trajectory and the velocity. The following figures 5.1 and 5.2 are each a composite of a calibration image (with stars) and some of the event image. It can be seen the brighter stars like Sirius, Betelgeuse, Procyon and the fireball trajectory.

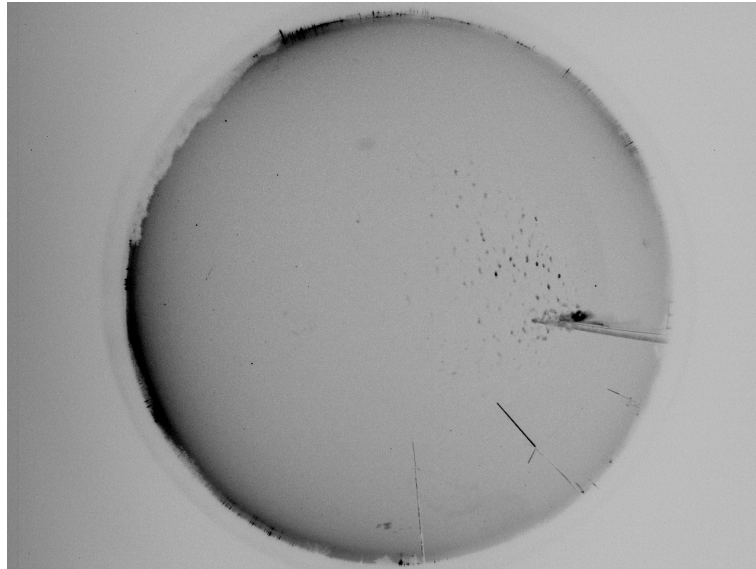


Figure 5.1: The figure is a composite of the fireball images with a calibration image that shows the brighter stars in the field of view and the trajectory of the fireball from the camera of Torino

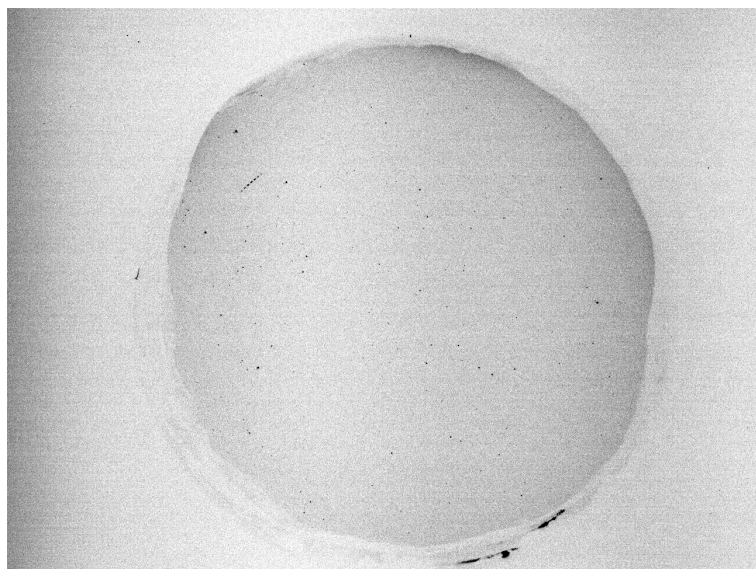


Figure 5.2: The figure is a composite of the fireball images with a calibration image that shows the brighter stars in the field of view and the trajectory of the fireball from the camera of Lignan.

As said the algorithm needs in input the geographical coordinates of the two stations, the mean time which the bolide appeared in and the calculated positions on the celestial sphere. Therefore an input file has been created for each station, as in table 5.1. The computation has been done for three point of the trajectory, the beginning when the fireball was visible, a mean point and the end of the luminous trajectory.

deltaT(s)	RA (deg)	DEC (deg)	deltaT(s)	RA (deg)	DEC (deg)
0.0000	83.7	+21.92	0.0	108.75	-1.01
0.1334	81.3	+22.95	0.2	105.62	+0.16
0.2667	78.4	+23.7	0.4	102.00	-1.37

Table 5.1: The two tables show the input file used for the two camera (to the left Torino, to the right Lignan) in order to compute the mean trajectory and the velocity of the fireball

In output the computation give a summary of the triangulation results for each camera, table 5.2.

Time (s)	Xgeotrc (km)	Ygeotrc (km)	Zgeotrc (km)
0.0000	-3932.6611	2347.4854	4547.3579
0.2000	-3921.9625	2342.7334	4550.5227
0.4000	-3910.8691	2337.8061	4553.8044
Lat (deg)	Long (deg)	Height (km)	V (km/s)
6.1097	44.9849	86.5723	60.6338
6.0921	45.0778	80.5980	62.8713
6.0738	45.1743	74.4214	62.8713

Time (s)	Xgeotrc (km)	Ygeotrc (km)	Zgeotrc (km)
0.0000	-3926.1119	2344.5765	4549.2953
0.1334	-3920.2175	2341.9584	4551.0389
0.2667	-3913.6230	2339.0293	4552.9897
Lat (deg)	Long (deg)	Height (km)	V (km/s)
6.0989	45.0417	82.9130	50.0840
6.0892	45.0929	79.6252	56.0750
6.0783	45.1503	75.9530	56.0750

Table 5.2: The first table shows the output file for the station of Lignan while the second table shows the output file for the station of Torino.

As result it has been obtained that the fireball seen by the cameras of Lignan and Torino has passed over France, near the vertical of Grenoble. The figure 5.3

shows the points of beginning, centre and end of the fireball measured by the two stations, projected onto the Earth's surface.

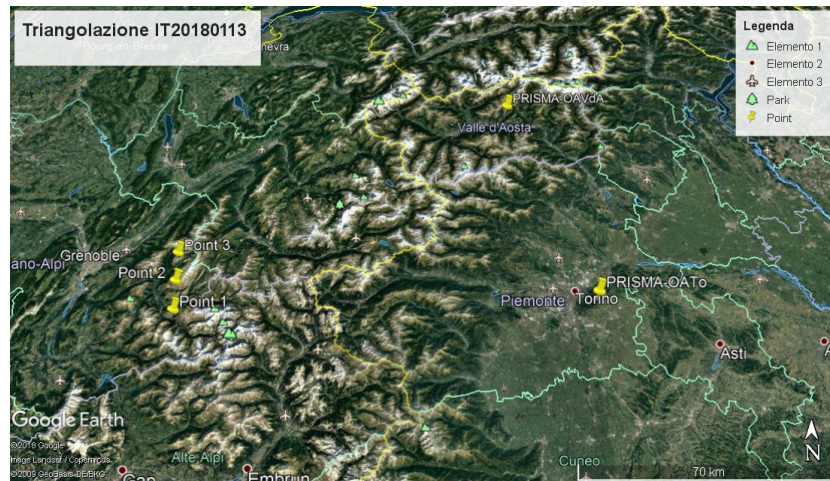
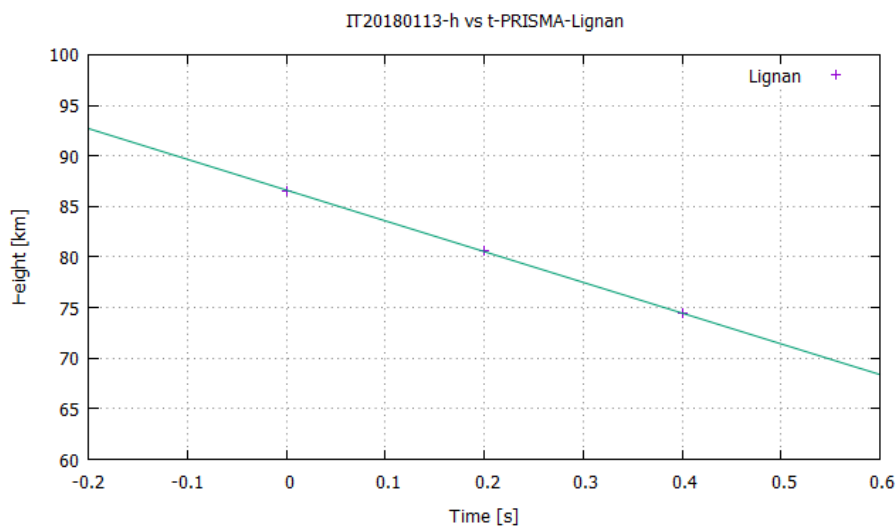


Figure 5.3: The figure shows the projection of the points of the fireball seen by the stations of Lignan and Torino with google maps.

The inclination of the trajectory onto the Earth's surface was of about 30° and azimuth of about 172° , so as it can be seen also in the previous figure 5.1, the fireball direction was going from south to north. The following plots has been obtained as results from the values of height versus time, figure 5.4.



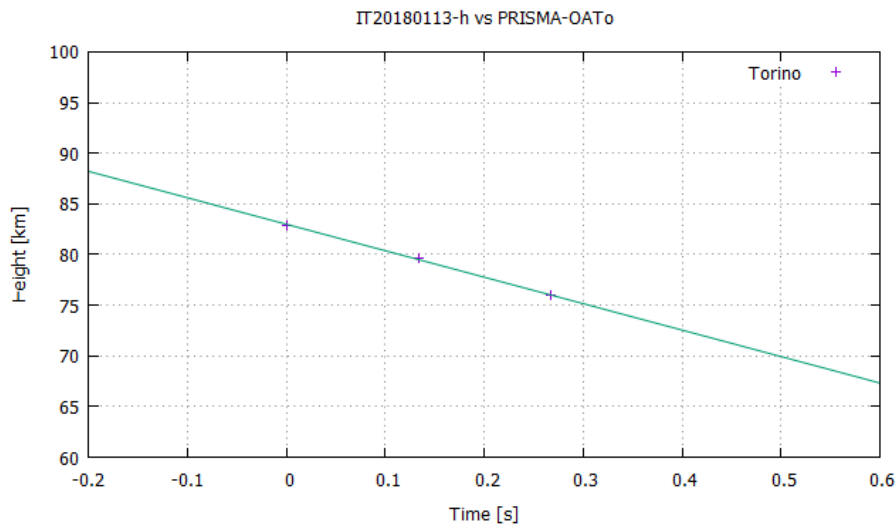


Figure 5.4: The figure shows two plots of obtained data for each station. Both plots shows in x axis the Time in seconds and in y axis the Height in km/s. The fit is has the same trend which indicates that over time the height decreases.

In these plots it can be observed that over time the height decreases and this is obviously the trend that it has to be expected from a fireball. With the velocity obtained for each point of the trajectory of the fireball then it has been computed the mean velocity with its error. Since the output values for the velocity are affected by the error of the astrometric solution, below it is reported the mean velocity obtained, 58.102 ± 4.553 km/s.

5.2.1 Conclusion and future prospective

There are different methods to approach the astrometry of a fireball observed with fish-eye cameras. The procedure used in this thesis has had as goal to study and replicate the pipeline used from FRIPON, in order to one day create a solid and independent Italian pipeline. To use this procedure in the first place, several calibration images as clean as possible are needed to extract catalogs that have a solid number of stars to be matched by Scamp. In fact, the main problem is to extract the catalogs from the best clean calibration images, that it is quite difficult since the calibration images seem to have a high background noise, given by artificial sources. This translates into error in minutes that has been obtained at the end of the run with Scamp. And then it propagates in a much significant error in the computation of the points of the trajectory and the mean velocity. But despite the consistent error in km/s, the solution which I arrived at it can be considered acceptable as a first approach. As future goals, naturally I intend to improve the procedure to achieve better results, primarily increasing the number of calibration images covering a longer period of time. Hence increasing the precision of the input coordinates I expect to reach a better triangulation and go on with the computation of the dynamic characterizations, such as orbit, dark flight and impact area.

Acknowledgements

I would like to thank Alberto Buzzoni to give the possibility to work with him in this project and teach me the real work of a researcher. To have always been there for me, I will always thank Albino Carbognani from the bottom of my heart. A special thank you to Chiara Marmo that has passed her knowledge about Sextractor and Scamp even if we never met personally. A thank you to Roberto Di Luca, he has supported me in the first part of my thesis and with Marco Lolli have help me greatly. THANK YOU in capitol letter to my family that has supported me through all my life, more and more in this adventure. And last by surely not the least I would like to thank my love that standed by me in up and down moments. Thank you all, I'm really greatful.

List of Figures

3.1	The figure shows a map of the PRISMA stations (red working, orange in setup phase and yellow still to buy) and the FRIPON station (blue)	21
3.2	acA1300-30gm Basler Camera	22
3.3	Loiano camera PRISMA	23
3.4	The spectral response curve taken from the user manual of Basler camera.	25
3.5	Masterdarks related to exposure times of 1, 2, 4 and 5 sec. On y-axis there is the logarithm of standard deviation and on x-axis there's the temperature	26
3.6	Masterbias related to exposure times of 1, 2, 4 and 5 sec. On y-axis there is the logarithm of standard deviation and on x-axis there's the temperature	27
3.7	This figure shows an image of Perseids' shower of 12 August 2017 taken from the station of Bologna. It cannot be seen the shower in this image because it has been chosen to perform the photometry only on stellar images, without meteoric phenomena.	28
3.8	Strumental magnitudes vs Catalog magnitudes in band B,V,R,I	32
3.9	ΔMag_{oss} vs $Color_{cat}$ in band B,V,R,I	34
3.10	Mag_{oss} vs Mag_{cat} in band B,V,R,I	36
3.11	Example of trend of rms in band B	37
4.1	This figure shows the pseudo dark median.	39
4.2	To the left it can be seen an example of a raw calibration image, to the right an example of a cleaned calibration image taken with the PRISMA camera of Lignan.	39
4.3	This figure shows a diagram taken from the manual of SExtractor explaining all the main steps and also the many extra options over a simple run of SE.	41
4.4	An illustration of how works DEBLEND-NTHRESH and DEBLEND-MINCONT	44

4.5	The figure shows an example of mask applied through SExtractor to the images.	46
4.6	The figure shows an example of the four apertures that SExtractor can applied in the process of photometry.	49
4.7	This is an example of check image of the extraction of stars from a calibration image of Lignan station. It can be observed how and what sextractor has extracted as objects. In particular the points darker are the objects extracted, the points like at the right bottom are artificial objects while the puntiform points fainter are the bad pixel.	51
4.8	This is an example of a file of parameter, default.param, used in this work. It is a list of parameters chosen to be calculated and written in the output catalog.	58
4.9	The figure shows which steps scamp undergoes to arrive at an astrometric and photometric solution.	59
4.10	This is a chart showing for each astrometric instrument an astrometric model of the input frame(s) after calibration. The pixel size is represented over the field of view using a colour scale ranging from blue to red.	67
4.11	The figure shows the file .aheader used for the first run of Scamp. The CRPIXs are the parameters indicating the center of the image in pixels, while CDs are the parameters related to the scale.	69
4.12	The figure shows part of the results when scamp is run the first time.	69
4.13	In the figure χ^2 of the internal catalog and the reference are compared, it can be seen that in general both values fluctuate about 200 and 800.	70
4.14	In the figure it is shown the application of the astrometric solution to a calibration image to verify that the stars are well recognized. The cursor points alpha Ursa Maior. Moreover it is verified that the orientation of the axis is so that North point south and East towards right.	71
5.1	The figure is a composite of the fireball images with a calibration image that shows the brighter stars in the field of view and the trajectory of the fireball from the camera of Torino	76
5.2	The figure is a composite of the fireball images with a calibration image that shows the brighter stars in the field of view and the trajectory of the fireball from the camera of Lignan.	76
5.3	The figure shows the projection of the points of the fireball seen by the station of Lignan and Torino with google maps.	78

5.4 The figure shows two plots of obtained data for each station. Both plots shows in x axis the Time in seconds and in y axis the Height in km/s. The fit is has the same trend which indicates that over time the height decreases. 79

Bibliography

- [1] Z. Ceplecha and J. Borovička, "Meteor Phenomena and Bodies", Space Science Reviews 84: 327-471, 1998
- [2] Dr. Benne W. Holwerda, Source Extractor for Dummies
- [3] E. Bertin, SExtractor v.2.13 User's manual
- [4] Bertin E., 2006, in Astronomical Data Analysis Software and System XV, ASP conf. Series 351, 112
- [5] "This research has made use of the VizieR catalog access tool, CDS, Strasbourg, France"
- [6] Z. Ceplecha, Geometric, Dynamic, Orbital and Photometric data on meteoroids from photographic fireball networks, 1987
- [7] M.R. Calabretta and E.W. Greisen, Representations of celestial coordinates in FITS, AA 395, 1077-1022 (2002)
- [8] E.W. Greisen and M.R. Calabretta, Representations of world coordinates in FITS, AA 395, 1061-1075 (2002)

Sitography

- [9] <http://www.prisma.inaf.it/index.php/il-progetto/>
- [10] <http://www.eso.org/sci/software/esomidas//>
- [11] <http://www.softpedia.com/get/Science-CAD/AstroImageJ.shtml>
- [12] <http://www.heavens-above.com/>
- [13] <http://www.sat.belastro.net/heavensat.ru/english/index.html>
- [14] <http://simbad.u-strasbg.fr/simbad/> astronnet <https://www.astromatic.net/>